https://doi.org/10.5194/hess-2020-586
Preprint. Discussion started: 10 December 2020

Hydrology and Earth System Sciences
Open Access
Discussions

Three-dimensional transient flow to a partially penetrated well with variable discharge in a general three-layer aquifer system

Qinggao Feng[1]*, Xiaola Feng[1], Hongbin Zhan[2]*

[1]Faculty of Engineering, China University of Geosciences, Wuhan, Hubei, 200092, P. R. China

[2]Department of Geology and Geophysics, Texas A&M University, College Station, TX 77843-3115, USA.

*Corresponding authors

Emails: fengqg@cug.edu.cn (Q. Feng), zhan@geos.tamu.edu (H. Zhan)

https://doi.org/10.5194/hess-2020-586
Preprint. Discussion started: 10 December 2020

Hydrology and Earth System Sciences
Discussions

ABSTRACT

A general analytical model for three-dimensional flow in a three-layered aquifer system with a partial penetration well having a variable discharge of pumping is developed by taking account of the interface flow on the adjacent layers. This general three-layer system includes the conventional aquitard-aquifer-aquitard system as a subset and does not require that the permeability contrasts of different layers must be greater than a few orders of magnitude, and does not ignore any flow components (either vertical or horizontal) in any particular layer. The pumping well of infinitesimal radius is screened at any portion of the middle layer. Three widely used top and bottom boundary conditions are considered that can be specified as a constant-head boundary (Case1) or a no-flux boundary (Case 2), and a constant-head boundary at the top in combination with a no-flux boundary at the bottom (Case 3). Laplace domain solutions for dimensionless drawdown are obtained by the use of Hankel transformation, and associated time-domain solutions are evaluated numerically. The newly obtained solutions include some available solutions for two- or single-layer aquifer systems as subsets. The drawdowns for individual layers caused by a well with an exponentially decreased discharge are explored as an example of illustration. The results indicate that the pumped layer drawdown close to the partially penetrated well is mainly influenced by the variable pumping rate. The late-time drawdowns for all layers are remarkably affected by the chosen types of top and bottom boundary conditions, and the drawdown for Case 3 is greater than that for Case 1 and smaller than that for Case 2. Additionally, the effect of the pumped layer anisotropy on drawdowns in the three-layer system is significant, and the anisotropy of the unpumped layers significantly affects the drawdown in the whole aquifer system without

https://doi.org/10.5194/hess-2020-586
Preprint. Discussion started: 10 December 2020

large contrast of hydraulic conductivity between the unpumped layers and the pumped layer. The drawdowns in all three layers are greatly affected by the location and length of well screen, and a larger drawdown can be seen at the position that is closer to the middle point of the screen of the partially penetrating pumping well.

Keywords: Three-layer system; Well partial penetration; Variable discharge; Top and bottom boundary; Semi-analytical solution.

https://doi.org/10.5194/hess-2020-586
Preprint. Discussion started: 10 December 2020

Hydrology and Earth System Sciences Discussions

1. **Introduction**

Most groundwater flow model concerning a pumping and/or injection well will have the pumping and observation wells in the same aquifer (Yeh and Chang, 2013; Houben, 2015). For a multi-aquifer system, the pumping and observation wells may be in the same aquifer or in different aquifers. As different aquifers in a multi-aquifer system are hydraulically connected, pumping in a specific aquifer will inevitably induce hydraulic responses over the entire multi-aquifer system, and the observation well in an unpumped aquifer will also record the drawdown information associated with pumping in the pumped aquifer. Therefore, the questions we need to answer are: How to interpret the drawdown information collected at an unpumped aquifer from the pumped aquifer? And furthermore, is that feasible to conduct aquifer characterization and to obtain the aquifer hydraulic parameters when the drawdown information is collected at an unpumped aquifer from the pumped aquifer? To answer these questions, one must first develop a robust groundwater flow model in a fully coupled multi-aquifer system. Unfortunately, the present models on this subject are severely limited to some demanding and often time unrealistic restrictions.

The present groundwater flow models related to multi-layer aquifer systems are usually established by solving the coupled partial differential equation group of groundwater flow explicitly or with a matrix solver (Bakker, 2013; Chen and Morohunfola, 1993; Cihan et al., 2011; Hantush, 1967; Hunt, 2005; Meonch, 1985; Neuman and Witherspoon, 1969). In those models, some strong assumptions are often invoked to simplify the system. For instance, it is commonly assumed that the permeability contrasts among two adjacent aquifers are more than a few orders of magnitude, thus flow in the much less permeable layer is assumed to be perpendicular to the layering while the flow in the much greater permeability layer is assumed to be parallel to the layering (Hantush, 1967; Neuman and Witherspoon, 1969). Such a simplification may be acceptable for investigating an aquifer-aquitard system as the aquitard/aquifer permeability contrasts can be indeed as large as a few orders of magnitude (Hantush, 1964; Lin et al., 2019; Neuman, 1968; Yeh and Chang, 2013). But this assumption is baseless for a general multi-aquifer system in which the permeability contrasts among different layers are much modest. Another commonly used assumption in present models is that mass exchange between two adjacent aquifers can be treated as a volumetric sink/source incorporated into the governing equations of flow in each individual layer (the so-called Hantush-Jacob assumption) (Hantush and Jacob, 1955). This assumption is also problematic in the sense that it does not honor the fact that mass exchange between two adjacent layers always occurs at the interfaces of those adjacent layers rather than as a volumetric sink/source inside those layers, a treatment that can generate considerable errors, as documented in numerous investigations (e.g. Hantush, 1967; Feng and Zhan, 2015; Feng et al., 2019, 2020; Zhan and Bian, 2006). A third simplification in present models is to assume a constant pumping rate (Hantush, 1964; Yeh and Chang, 2013). The constant pumping rate is desirable but is quite difficult to maintain in actual pumping scenarios which almost always involve variable pumping rates because of many reasons such as the temporary loss of power, increased drawdown in the pumping well with time (which makes it more difficult to lift water from the pumping well) and other constrains in conducting pumping tests in the field (Chen et al., 2020; Hantush, 1964; Mishra et al., 2013; Sen and Altunkaynak, 2004; Singh, 2009; Wen et al., 2017).

In theory, numerical modeling can avoid many restrictions mentioned above to investigate a multi-aquifer system, but it has some issues that are sometimes not easy to resolve. For instance, it is not straightforward to use a numerical model for aquifer characterization to obtain the aquifer parameters, particularly when dealing with a multi-aquifer system involving many hydraulic parameters for multiple aquifers. When the numerical model has to be used for such a purpose, it often involves either trial-and-error or automatic optimization procedures to minimize the model-generated drawdown with the observed drawdown (Mohanty et al., 2013; Jeong and Park; 2019; Rajaee, et al., 2019). This process can sometimes lead to non-uniqueness of inverted aquifer parameters (Rahman et al., 2020). Another issue associated with numerical model is that without a benchmark analytical solution, it is unknown how much numerical errors have been involved in the numerical model. For a multi-aquifer system, the numerical errors can be considerable near the interfaces of different aquifers where the aquifer parameters change suddenly (Neuman, 1968; Louwyck et al., 2012). If one recalls that any numerical approaches (no matter they are finite-difference, finite-element, boundary-element, or others) essentially involve some sorts of smoothing or average schemes to approximate the mass conservation law in a discrete sense, then it is not surprise to know that numerical errors are prone to be large near sharp interfaces (Cihan et al., 2011; Neuman, 1968; Li and Neuman, 2007; Loudyi et al., 2007). Of course, one can use gradually finer meshes when approaching the interfaces of different aquifers to minimize the numerical errors, but such a procedure can sometimes increase the computational cost rapidly, particularly when dealing with three-dimensional (3D) flow in a multi-aquifer system (Feng et al., 2020; Rajaee, et al., 2019; Rahman et al., 2020; Rühaak et

https://doi.org/10.5194/hess-2020-586
Preprint. Discussion started: 10 December 2020

al., 2008). Overall, establishing a sufficiently accurate numerical model for groundwater flow in a multi-aquifer system is feasible, but often time requires considerable preparations and computational cost.

Based on above considerations, we are going to establish a robust and generic 3D groundwater flow in a three-aquifer system in this investigation. The generality of this work is reflected on the following aspects. Firstly, it does not put any constrains on the permeability contrasts among different aquifers involved. Such a generality will make this work much more appealing to deal with a vast number of cases in actual aquifer setting. It also encompasses previous aquifer-aquitard two-layer system and aquitard-aquifer-aquitard three-layer systems as subsets. It can even be applied for an extreme two-layer or three-layer system such as a fracture-rock two-layer system or a rock-fracture-rock three-layer system when flow can occur in both fractures and rock matrix. Furthermore, for the rock-fracture-rock three-layer system, the rocks adjacent to the fracture can be either identical with the same hydraulic properties or have different lithology and hydraulic properties. The two-aquifer system investigated by Feng et al. (2019) is also a subset of this study. Secondly, this study honors the mass exchange among different aquifers as an interface flow phenomenon, not as a volumetric sink/source term, as in the Hantush-Jacob assumption. Thirdly, the pumping rate can be any given function of time instead of being a constant. This is a distinctive difference from the three-aquifer study of Feng et al. (2020) involving constant pumping rate. Fourthly, three widely used top and bottom boundary conditions are considered that can be specified as a constant-head boundary (Case1) or a no-flux boundary (Case 2), and a constant-head boundary at the top in combination with a no-flux boundary at

https://doi.org/10.5194/hess-2020-586
Preprint. Discussion started: 10 December 2020

Hydrology and Earth System Sciences
Discussions
Open Access

the bottom (Case 3). This is also in contrast with Feng et al. (2019, 2020) which cannot investigate the combined effects of the top and bottom boundaries simultaneously. In the following sections, semi-analytical drawdown solutions in nondimensional forms in a genetic three-layer system are obtained by performing Laplace-Hankel transform and eventually the real time solutions are calculated by the method of numerical inversion. Finally, as an example of illustration, the characteristics of drawdown are thoroughly investigated due to a partially penetrated well pumped at an exponentially decreased discharge function. The results are discussed extensively and their applications are elaborated as well.

2. Methodology

2.1 Mathematical model

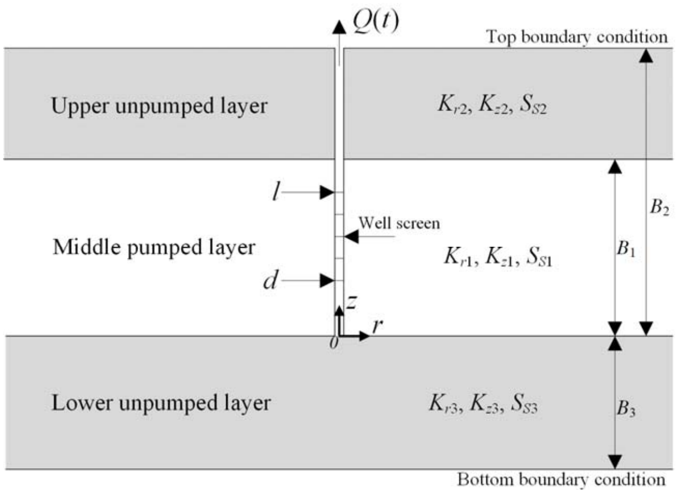

Fig.1 Schematic diagram of a three-layer aquifer system with a partial penetration well

Fig. 1 displays an infinitesimal-radius well with a variable discharge $Q(t)$ in a general three-layer aquifer system of unbound lateral extension. The pumping well is partially penetrated in the middle layer of the system with a screen length from d to l shown in this figure. Each layer of constant thickness is homogeneous and anisotropic. Three-dimensional flow is included in all layers. The interface flow at the two neighboring layers is linked with head and flux continuity conditions. It is noted that three different cases presented by Hantush (1960) are concluded, specifically, the boundaries at the top and bottom are simultaneously constant-head boundaries (Case 1), no-flux boundaries (Case 2), or a combination of a constant-head top boundary and no-flux bottom boundary (Case 3). The cylindrical coordinate origin is at the intersection of the well axis and the bottom of the middle-pumped layer.

According to the conceptual model above, the equations that govern the transient drawdown distribution for flow to a pumping well can be given by:

$$\frac{K_{ri}}{r}\frac{\partial}{\partial r}\left(r\frac{\partial s_i(r,z,t)}{\partial r}\right)+K_{zi}\frac{\partial^2 s_i(r,z,t)}{\partial z^2}=S_{si}\frac{\partial s_i(r,z,t)}{\partial t} \quad (1)$$

where s (r, z, t) denotes drawdown at space coordinate (radial distance r [L], vertical distance z [L]) and time coordinate (pumping time t [L]); K_r and K_z indicate, respectively, the hydraulic conductivities in the radial and vertical direction [L/T]; S_s refers to specific storage [1/L], and $i = 1, 2, 3$ designate, respectively, the middle-pumped layer, upper layer and lower layer.

The initial conditions of the aquifer system can be written as:

$$s_i(r,z,0)=0 \quad (2)$$

The boundary of the aquifer system at infinity yields:

$$s_i(\infty,z,t)=0 \quad (3)$$

The pumping well of infinitesimal diameter is partially penetrated in the middle layer, the wellbore boundary condition is subject to (Hantush, 1964, Liang et al, 2018):

https://doi.org/10.5194/hess-2020-586
Preprint. Discussion started: 10 December 2020

$$\lim_{r \to 0} r \frac{\partial s_1}{\partial r} = \begin{cases} 0 & l < z \le B_1 \\ -\dfrac{Q(t)}{2\pi K_{r,1}(l-d)} & d \le z \le l \\ 0 & 0 \le z < d \end{cases} \quad (4)$$

in which $Q(t)$ represents the well discharge of pumping [L^3T^{-1}], B_1 refers to the thickness of the middle-pumped aquifer [L]. It is notable that an assumption of the well discharge uniformly distributed along the screened section of the partially penetrating well is used herein. This, of course, is a simplification for the sake of mathematical modeling. Fortunately, this simplification is proven to be sufficiently accurate for regions that are not extremely close to the pumping well (within a few well radii) (Chang and Yeh, 2013).

As an example of illustration, the pumping rate used in this study varies exponentially with the pumping time in the form (Hantush, 1964b, 1966; Wen et al., 2017):

$$Q(t) = Q + (Q_1 - Q)e^{-\alpha t} \quad (5)$$

which is based on lots of field data and available works (Chen et al., 2020; Feng et al., 2019; Sen and Altunkaynak, 2004). The symbol Q and Q_1 represent the final (constant) and initial well discharge, respectively [L^3T^{-1}], and α designates decay constant obtained from the measured data of pumping [T^{-1}].

The inner well-face boundary conditions at the upper and lower unpumped layers yield:

$$\lim_{r \to 0} r \frac{\partial s_2}{\partial r} = \lim_{r \to 0} r \frac{\partial s_3}{\partial r} = 0 \quad (6)$$

And the boundary condition at the interface between the middle-pumped aquifer and the adjacent upper layer ($z = B_1$) requires that:

$$s_1(r,z,t) = s_2(r,z,t), \quad z = B_1 \quad (7)$$

and

https://doi.org/10.5194/hess-2020-586
Preprint. Discussion started: 10 December 2020

$$K_{z,1}\frac{\partial s_1(r,z,t)}{\partial z}=K_{z,2}\frac{\partial s_2(r,z,t)}{\partial z},\ \ z=B_1 \quad (8)$$

The continuity of hydraulic connection between the middle-pumped layer and the lower unpumped layer (z = 0) can be written as:

$$s_1(r,z,t)=s_3(r,z,t),\ \ z=0 \quad (9)$$

and

$$K_{z1}\frac{\partial s_1(r,z,t)}{\partial z}=K_{z3}\frac{\partial s_3(r,z,t)}{\partial z},\ \ z=0 \quad (10)$$

The top boundary condition at the upper unpumped layer ($z = B_2$) and the bottom boundary condition at the lower unpumped layer ($z = B_3$) of the aquifer system can be, in the manner of Hantush (1960) and Moench (1985), expressed in three ways.

For Case 1, the constant-head boundaries at both top and bottom boundaries can be respectively written as

$$s_2(r,z,t)=0,\ \ z=B_2 \quad (11)$$

and

$$s_3(r,z,t)=0,\ \ z=-B_3 \quad (12)$$

For Case 2, the no-flux boundary at both top and bottom boundaries yield

$$\frac{\partial s_2(r,z,t)}{\partial z}=0,\ \ z=B_2 \quad (13)$$

and

$$\frac{\partial s_3(r,z,t)}{\partial z}=0,\ \ z=-B_3 \quad (14)$$

For Case 3, the constant-head boundary at the top and the no-flux boundary at the bottom are respectively

$$s_2(r,z,t)=0,\ \ z=B_2 \quad (15)$$

and

https://doi.org/10.5194/hess-2020-586
Preprint. Discussion started: 10 December 2020

Hydrology and Earth System Sciences
Discussions

$$\frac{\partial s_3(r,z,t)}{\partial z}=0,\ z=-B_3 \quad (16)$$

It should be remarked that the adopted three different types of top and bottom boundaries expressed in Eqs. (11)–(16) are commonly encountered in practice. In some cases, the upper layer is covered with ponded water, the upper and lower layers are, respectively, overlain and underlain a layer of a highly transmissivity, or the induced drawdown at the top/bottom boundary is not affected by pumping. Under such conditions, the constant-head condition can be imposed at the boundary. On the other hand, if there is an impermeable layer below the lower layer or above the upper layer, the no-flux boundary can be adopted correspondingly. As for the relevant literature, one may consult Baker (2006), Chen et al. (2020), Feng et al. (2019, 2020), Feng and Zhan (2015, 2016, 2019), Hantush (1960, 1964), Hemker and Maas (1987), Hunt (2005), Moehch (1985), Neuman and Witherspoon (1969), Sepúlveda (2008), Wang et al. (2015) and Wen et al. (2011, 2013).

2.2 Dimensionless solutions

2.2.1 Dimensionless equations

Table 1 Dimensionless variables and parameters

$r_D=r/B_1$	$\alpha_{ri}=K_{ri}/S_{Si}$	$\gamma_1=\kappa_1\xi_2/\xi_1$
$l_D=l/B_1$	$\alpha_{zi}=K_{zi}/S_{Si}$	$\gamma_2=\kappa_2\xi_3/\xi_2$
$z_D=z/B_1$	$B_{D2}=B_2/B_1$	$s_{Di}=4\pi K_{r1}B_1 s_i/Q$
$d_D=d/B_1$	$B_{D3}=B_3/B_1$	$\alpha_D=\alpha S_{S1}B_1^2/K_{r1}$
$t_D=\alpha_{r1}t/B_1^2$	$\alpha_{Dri}=\alpha_{ri}/\alpha_{r1}$	$\xi_i^2=(\alpha_{Dri}\lambda^2+p)/\alpha_{Dzi}$
$\kappa_2=K_{z2}/K_{z1}$	$\alpha_{Dzi}=\alpha_{zi}/\alpha_{r1}$	$\theta_1=\xi_2\left(B_{D2}-1\right)+\xi_3 B_{D3}$
$Q_{1D}=Q_1/Q$	$\kappa_3=K_{z3}/K_{z2}$	$\theta_2=\xi_2\left(B_{D2}-1\right)-\xi_3 B_{D3}$

https://doi.org/10.5194/hess-2020-586
Preprint. Discussion started: 10 December 2020

Hydrology and Earth System Sciences
Discussions

When dealing with complex hydrodynamic systems such as this study, nondimensionalization has the advantage of untangling parameter correlation thus reducing the number of independent free parameters controlling the system, thus is employed here. Using the defined nondimensional variables listed in Table 1, Eqs. (1)-(16) become the following equations in the dimensionless forms as:

$$\alpha_{Dri}\left(\frac{\partial^2 s_{Di}}{\partial r_D^2}+\frac{1}{r_D}\frac{\partial s_{Di}}{\partial r_D}\right)+\alpha_{Dzi}\frac{\partial^2 s_{Di}}{\partial z_D^2}=\frac{\partial s_{Di}}{\partial t_D} \quad (17)$$

$$s_{Di}\left(r_D,z_D,0\right)=0 \quad (18)$$

$$s_{Di}\left(\infty,z_D,t_D\right)=0 \quad (19)$$

$$\lim_{r\to 0} r_D\frac{\partial s_{1D}}{\partial r_D}=\begin{cases}0 & l_D<z_D\le 1\\ -2\dfrac{Q_D\left(t_D\right)}{l_D-d_D} & d_D\le z_D\le l_D\\ 0 & 0\le z_D<d_D\end{cases} \quad (20)$$

$$Q\left(t_D\right)=1+\left(Q_{1D}-1\right)e^{-\alpha_D t_D} \quad (21)$$

$$\lim_{r_D\to 0} r_D\frac{\partial s_{D2}}{\partial r_D}=0 \quad (22)$$

$$\lim_{r_D\to 0} r_D\frac{\partial s_{D3}}{\partial r_D}=0 \quad (23)$$

$$s_{D1}\left(r_D,z_D,t_D\right)=s_{D2}\left(r_D,z_D,t_D\right),\quad z_D=1 \quad (24)$$

$$\frac{\partial s_{D1}\left(r_D,z_D,t_D\right)}{\partial z_D}=\kappa_1\frac{\partial s_{D2}\left(r_D,z_D,t_D\right)}{\partial z_D},\quad z_D=1 \quad (25)$$

$$s_{D1}\left(r_D,z_D,t_D\right)=s_{D3}\left(r_D,z_D,t_D\right),\quad z_D=0 \quad (26)$$

$$\frac{\partial s_{D1}\left(r_D,z_D,t_D\right)}{\partial z_D}=\kappa_2\frac{\partial s_{D3}\left(r_D,z_D,t_D\right)}{\partial z_D},\quad z_D=0 \quad (27)$$

Case 1,

$$s_{D2}\left(r_D,z_D,t_D\right)=0,\quad z_D=B_{D2} \quad (28)$$

$$s_{D3}\left(r_D,z_D,t_D\right)=0,\quad z=-B_{D3} \quad (29)$$

Case 2,

https://doi.org/10.5194/hess-2020-586
Preprint. Discussion started: 10 December 2020

Hydrology and Earth System Sciences
Open Access
Discussions

$$\frac{\partial s_{D2}(r_D,z_D,t_D)}{\partial z} = 0,\ \ z_D = B_{D2} \quad (30)$$

$$\frac{\partial s_{D3}(r_D,z_D,t_D)}{\partial z_D} = 0,\ \ z_D = -B_{D3} \quad (31)$$

Case 3,

$$s_{D2}(r_D,z_D,t_D) = 0,\ \ z_D = B_{D2} \quad (32)$$

$$\frac{\partial s_{D3}(r_D,z_D,t_D)}{\partial z_D} = 0,\ \ z_D = -B_{D3} \quad (33)$$

in which the subscript ‘ D ’ designates nondimensional terms.

2.2.2 Dimensionless solutions for Case 1

With the help of the constant-head boundary at the top and bottom expressed in Eqs. (28) and (29), the drawdown solutions in the three layers can be derived by performing Laplace-Hankel transform, the detailed derivations are shown in Appendix A.

The dimensionless drawdown for the middle-pumped layer in Laplace space yields

$$\bar{s}_{D1} = \int_0^\infty \left\{\hat{\bar{u}}_D(\lambda,z_D,p) - 4\left[\hat{\bar{u}}(r_D,0,p)\gamma_2 f_{11} + \hat{\bar{u}}(r_D,1,p)\gamma_1 f_{12}\right]/\chi_1\right\}\lambda J_0(\lambda r_D)\,d\lambda \quad (34a)$$

where

$$\hat{\bar{u}}_D(\lambda,z_D,p) = 2\frac{\cosh(\xi_1\zeta_D) - \delta\hat{\bar{u}}_D(\xi_1,z_D)}{\alpha_{Dz1}\xi_1^2(l_D-d_D)} \quad (34b)$$

$$\zeta_D = \begin{cases} z_D - l_D & l_D < z_D \le 1 \\ 0 & d_D \le z_D \le l_D \\ d_D - z_D & 0 \le z_D < d_D \end{cases} \quad (34c)$$

$$\delta\hat{\bar{u}}_D(\xi_1,z_D) = \frac{\sin\left[\xi_1(1-l_D)\right]\cosh(\xi_1 z_D) + \cosh\left[\xi_1(1-z_D)\right]\sinh(\xi_1 d_D)}{\sinh(\xi_1)} \quad (34d)$$

$$f_{11} = \sinh\left[\xi_1(1-z_D)\right](\cosh\theta_1 + \cosh\theta_2)\gamma_1 + \cosh\left[\xi_1(1-z_D)\right](\sinh\theta_1 + \sinh\theta_2) \quad (34e)$$

$$f_{12} = \sinh(\xi_1 z_D)(\cosh\theta_1 + \cosh\theta_2)\gamma_2 + \cosh(\xi_1 z_D)(\sinh\theta_1 - \sinh\theta_2) \quad (34f)$$

$$\begin{aligned}\chi_1 &= 2(1+\gamma_1)(1+\gamma_2)\sinh(\xi_1+\theta_1) + 2(1-\gamma_1)(1-\gamma_2)\sinh(\xi_1-\theta_1) \\ &\quad -2(1+\gamma_1)(1-\gamma_2)\sinh(\xi_1+\theta_2) - 2(1-\gamma_1)(1+\gamma_2)\sinh(\xi_1-\theta_2)\end{aligned} \quad (34g)$$

in which $J_0(\cdot)$ represents the zero-order and first kind Bessel function, p and λ refer,

https://doi.org/10.5194/hess-2020-586
Preprint. Discussion started: 10 December 2020

respectively, to the variables of the transformations of Laplace and Hankel, and, accordingly, over bar and over hat sign indicate , respectively, the Laplace and Hankel domain parameter, $\hat{\bar{u}}_D$ provided by Feng et al. (2019) indicates the Hantush (1964) solution in Laplace-Hankel domain for a partially penetration well with variable discharge in a single confined aquifer.

The dimensionless solution of drawdown in the upper unpumped layer yields

$$\bar{s}_{D2} = 8\int_0^\infty \frac{\sinh\left[\xi_2\left(B_{D2}-z_D\right)\right]}{\chi_1}\cosh\left(\xi_3 B_{D3}\right)\left\{\hat{\bar{u}}\left(r_D,0,p\right)\gamma_2 - \hat{\bar{u}}\left(r_D,1,p\right)\left[\gamma_2\cosh\left(\xi_1\right)+\sinh\left(\xi_1\right)\right]\right\}\lambda J_0\left(\lambda r_D\right) \quad (35)$$

The semi-analytical solution of dimensionless drawdown in the lower unpumped layer is written as

$$\bar{s}_{D3} = 8\int_0^\infty \frac{\sinh\left[\xi_3\left(B_{D3}+z_D\right)\right]}{\chi_1}\left\{\hat{\bar{u}}\left(r_D,0,p\right)g_{31} - \hat{\bar{u}}\left(r_D,1,p\right)\gamma_1\cosh\left[\xi_2\left(B_{D2}-1\right)\right]\right\}\lambda J_0\left(\lambda r_D\right)d\lambda \quad (36a)$$

where

$$g_{31} = \gamma_1\cosh\left[\xi_2\left(B_{D2}-1\right)\right]\cosh\xi_1 + \sinh\left[\xi_2\left(B_{D2}-1\right)\right]\sinh\xi_1 \quad (36b)$$

2.2.3 Dimensionless solutions for Case 2

If the boundaries at the top and bottom of the aquifer system satisfy the no-flux boundary written in Eqs.(30)-(31), one can follow the procedures listed in Appendix A and develop the semi-analytical solutions of dimensionless drawdown in individual layer of the three-layer aquifer system. The drawdown solution in Laplace-domain in the middle-pumped layer yields

$$\hat{\bar{s}}_{D1} = \int_0^\infty\left\{\hat{\bar{u}}_D\left(\lambda,z_D,p\right)+4\left[\hat{\bar{u}}\left(r_D,0,p\right)\gamma_2 f_{21}+\hat{\bar{u}}\left(r_D,1,p\right)\gamma_1 f_{22}\right]/\chi_2\right\}\lambda J_0\left(\lambda r_D\right)d\lambda \quad (37a)$$

where

$$f_{21} = -\sinh\left[\xi_1\left(1-z_D\right)\right]\left(\cosh\theta_2-\cosh\theta_1\right)\gamma_1+\cosh\left[\xi_1\left(1-z_D\right)\right]\left(\sinh\theta_1-\sinh\theta_2\right) \quad (37b)$$

$$f_{22} = \sinh\left(\xi_1 z_D\right)\left(\cosh\theta_1-\cosh\theta_2\right)\gamma_2+\cosh\left(\xi_1 z_D\right)\left(\sinh\theta_1+\sinh\theta_2\right) \quad (37c)$$

https://doi.org/10.5194/hess-2020-586
Preprint. Discussion started: 10 December 2020

$$\begin{aligned}\chi_2 = &-2(1+\gamma_1)(1+\gamma_2)\sinh(\xi_1+\theta_1)-2(1-\gamma_1)(1-\gamma_2)\sinh(\xi_1-\theta_1)\\ &-2(1+\gamma_1)(1-\gamma_2)\sinh(\xi_1+\theta_2)-2(1-\gamma_1)(1+\gamma_2)\sinh(\xi_1-\theta_2)\end{aligned} \quad (37d)$$

The drawdown solution in Laplace domain in the upper unpumped layer yields

$$\bar{s}_{D2} = 8\int_0^\infty \frac{\cosh\left[\xi_2\left(B_{D2}-z_D\right)\right]}{\chi_2}\left[\gamma_2\sinh\left(\xi_3 B_{D3}\right)\hat{\bar{u}}\left(r_D,0,p\right)-\hat{\bar{u}}\left(r_D,1,p\right)M\right]\lambda J_0\left(\lambda r_D\right) \quad (38)$$

in which $M = \gamma_2\sinh(\xi_3 B_{D3})\cosh(\xi_1)+\cos(\xi_3 B_{D3})\sinh(\xi_1)$.

The drawdown solution in Laplace domain in the lower unpumped layer can be expressed as

$$\bar{s}_{D3} = 8\int_0^\infty \frac{\cosh\left[\xi_3\left(B_{D3}+z_D\right)\right]}{\chi_2}\left\{-\hat{\bar{u}}\left(r_D,0,p\right)g_{32}+\hat{\bar{u}}\left(r_D,1,p\right)\gamma_1\sinh\left[\xi_2\left(B_{D2}-1\right)\right]\right\}\lambda J_0\left(\lambda r_D\right) \quad (39a)$$

where

$$g_{32} = \gamma_1\sinh\left[\xi_2\left(B_{D2}-1\right)\right]\cosh\xi_1+\cosh\left[\xi_2\left(B_{D2}-1\right)\right]\sinh\xi_1 \quad (39b)$$

2.2.4 Dimensionless solutions for Case 3

By analogy, with the use of the constant-head boundary at the top and the no-flux boundary at the bottom, which are, respectively, described by Eq. (32) and Eq. (33), one can develop the nondimensional drawdown solutions in Laplace space for the middle (pumped) layer as:

$$\hat{\bar{s}}_{D1} = \hat{\bar{u}}_D\left(\lambda,z_D,p\right)+\frac{4}{\chi_3}\left[\hat{\bar{u}}\left(r_D,0,p\right)\gamma_2 f_{31}+\hat{\bar{u}}\left(r_D,1,p\right)\gamma_1 f_{32}\right] \quad (40a)$$

where

$$f_{31} = -\sinh\left[\xi_1\left(1-z_D\right)\right]\left(\sinh\theta_2-\sinh\theta_1\right)\gamma_1+\cosh\left[\xi_1\left(1-z_D\right)\right]\left(\sinh\theta_1-\sinh\theta_2\right) \quad (40b)$$

$$f_{32} = \sinh\left(\xi_1 z_D\right)\left(\sinh\theta_1-\sinh\theta_2\right)\gamma_2+\cosh\left(\xi_1 z_D\right)\left(\cosh\theta_1+\cosh\theta_2\right) \quad (40c)$$

$$\begin{aligned}\chi_3 = &-2(1+\gamma_1)(1+\gamma_2)\cosh(\xi_1+\theta_1)+2(1-\gamma_1)(1-\gamma_2)\cosh(\xi_1-\theta_1)\\ &-2(1+\gamma_1)(1-\gamma_2)\cosh(\xi_1+\theta_2)+2(1-\gamma_1)(1+\gamma_2)\cosh(\xi_1-\theta_2)\end{aligned} \quad (40d)$$

and, for the upper unpumped layer, one has

https://doi.org/10.5194/hess-2020-586
Preprint. Discussion started: 10 December 2020

Hydrology and Earth System Sciences Discussions

$$\bar{s}_{D2} = 8\int_0^\infty \frac{\sinh\left[\xi_2\left(B_{D2}-z_D\right)\right]}{\chi_3}\left[\gamma_2 \sinh\left(\xi_3 B_{D3}\right)\hat{\bar{u}}\left(r_D,0,p\right) - \hat{\bar{u}}\left(r_D,1,p\right)N\right]\lambda J_0\left(\lambda r_D\right) \quad (41)$$

in which $N = \gamma_2 \sinh(\xi_3 B_{D3})\cosh(\xi_1) + \cosh(\xi_3 B_{D3})\sinh(\xi_1)$.

and, for the lower pumped layer, one has

$$\bar{s}_{D3} = 8\int_0^\infty \frac{\cosh\left[\xi_3\left(B_{D3}+z_D\right)\right]}{\chi_3}\left\{-\hat{\bar{u}}\left(r_D,0,p\right)g_{33} + \hat{\bar{u}}\left(r_D,1,p\right)\gamma_1 \cosh\left[\xi_2\left(B_{D2}-1\right)\right]\right\}\lambda J_0\left(\lambda r_D\right) \quad (42a)$$

where

$$g_{33} = \gamma_1 \cos\left[\xi_2\left(B_{D2}-1\right)\right]\cosh\xi_1 + \sinh\left[\xi_2\left(B_{D2}-1\right)\right]\sinh\xi_1 \quad (42b)$$

2.3 Special cases

2.3.1 Special cases in a three-layer aquifer

If removing the effect of the radial flow in the upper and lower unpumped layer (K_{r2} = K_{r3} = 0, $\alpha_{r2} = \alpha_{Dr2} = 0$, $\alpha_{r3} = \alpha_{Dr3} = 0$, $\xi_2^2 = p/\alpha_{Dz2}$ and $\xi_3^2 = p/\alpha_{Dz3}$), the developed solutions of Eqs. (33) – (41) agree with the solutions for a conventional aquitard-aquifer-aquitard system with the assumption of only considering the vertical flows in the unpumped layers, as in previous works of Hantush (1960), Moench (1985) and Chen et al. (2020). The condition for this assumption is that the permeability of the middle-pumped aquifer is usually larger at least two orders of magnitude than that of the upper and lower aquitards.

Additionally, the transient dimensionless solutions in the three-layer aquifer system caused by a partially penetrating constant-rate pumping well in the middle layer can be obtained from Eqs. (34) – (42) by setting Q_{1D} = 1, and as far as the author knows, these solutions have not been developed in the existing studies.

2.3.2 Special cases in a two-layer aquifer

If the lower unpumped layer is absence, one has B_{D3} = 0, $\gamma_2 = 0$, and $\theta_1 = \theta_2 = \xi_2\left(B_{D2}-1\right)$,

https://doi.org/10.5194/hess-2020-586
Preprint. Discussion started: 10 December 2020

Hydrology and Earth System Sciences
Discussions

the dimensionless drawdown solutions in a two-layer aquifer having a constant-head and no-flow boundary at the top (Case 2 and Case3) can be, respectively, developed from Eqs. (37) – (42) and the detailed expression can be, respectively, given by:

Case 2: for the pumped layer, one has

$$\hat{\bar{s}}_{D1} = \hat{\bar{u}}_D(\lambda, z_D, p) + 2\frac{\hat{\bar{u}}(r_D, 1, p)}{\chi_2'}\gamma_1 \cosh(\xi_1 z_D)\sinh\left[\xi_2(B_{D2}-1)\right] \quad (43)$$

and for the upper unpumped layer, one has

$$\hat{\bar{s}}_{D2} = -2\frac{\hat{\bar{u}}(r_D, 1, p)}{\chi_2'}\cosh\left[\xi_2(B_{D2}-z_D)\right]\sinh(\xi_1) \quad (44)$$

with

$$\chi_2' = (\gamma_1 - 1)\sinh\left[\xi_1 - \xi_2(B_{D2}-1)\right] - (\gamma_1+1)\sinh\left[\xi_1 + \xi_2(B_{D2}-1)\right] \quad (45)$$

Case 3: for the pumped layer, one has

$$\hat{\bar{s}}_{D1} = \hat{\bar{u}}_D(\lambda, z_D, p) + 2\frac{\hat{\bar{u}}(r_D, 1, p)}{\chi_1}\gamma_1 \cosh\left[\xi_2(B_{D2}-1)\right]\cosh(\xi_1 z_D) \quad (46)$$

and for the upper unpumped layer, one has

$$\hat{\bar{s}}_{D2} = -2\frac{\hat{\bar{u}}(r_D, 1, p)}{\chi_3'}\sinh(\xi_1)\sinh\left[\xi_2(B_{D2}-z_D)\right] \quad (47)$$

with

$$\chi_3' = (1-\gamma_1)\cosh\left[\xi_1 - \xi_2(B_{D2}-1)\right] - (1+\gamma_1)\cosh\left[\xi_1 + \xi_2(B_{D2}-1)\right] \quad (48)$$

These solutions of drawdown agree with the solutions of Feng et al. (2019), describing flow in a two-layer aquifer system pumped by a partial penetration well of a variable/constant discharge subject to a zero-drawdown and no-flux conditions at the top boundary.

Further, if $Q_{1D} = 1$, $\alpha_{r2} = \alpha_{Dr2} = 0$ and $\xi_2^2 = p/\alpha_{Dz2}$, the drawdown solutions of Eqs. (43) – (45) are equal to the solutions having different expressions developed by Feng and Zhan (2015), that can be applied to investigate the drawdown caused by a pumping well of partial

https://doi.org/10.5194/hess-2020-586
Preprint. Discussion started: 10 December 2020

Hydrology and Earth System Sciences Discussions
Open Access EGU

penetration in an aquitard-aquifer system where the horizontal flow in the upper layer is neglected and a zero-drawdown condition can be imposed at the top boundary.

2.3.3 Special cases in a single-layer aquifer

If ignoring the leakage effect between two adjacent layers, the present pumped layer drawdown solutions can reduce to the solution of Hantush (1964) for flow in a confined aquifer due to a partially penetrated well with constant pumping rate (Q_{1D} = 1). When the pumped layer is fully penetrated by a well with an exponentially decreasing discharge and leakage is not considered, Eqs. (34b)–(34d) collapse to the drawdown solution of Wen et al. (2017). Additionally, the classical solution of Theis is also included in the new obtained solution when Q_{1D} = 1.

2.4 Numerical inversion of the solutions

So far, the Laplace-domain solutions of nondimensional drawdown for diverse cases are developed. In this study, a numerical integration algorithm (Ogata, 2005) with the method using the zeros of the Bessel functions as nodes can be performed to calculate the infinite integral associated with the transformation of Hankel, and the method of de Hoog algorithm (De Hoog et al., 1982) is able to be applied to solve the transformation of Laplace. Finally, one can obtain the solutions in time domain by successively using the two method of numerical inversion of Hankel transform and Laplace transform respectively. The verification and validation of the method have been proven and more details can be found in the study of Feng et al. (2020) and Liang et al. (2018), which is not discussed herein.

3 Results

The dimensionless drawdown response due to a partial penetration well pumped at an

https://doi.org/10.5194/hess-2020-586
Preprint. Discussion started: 10 December 2020

exponentially decreasing discharge is explored in the following from a number of perspectives. Default values for realistic aquifers are used in the following analysis: $B_1 = 20$m; $B_2 = 30$m; $B_3 = 10$m; $K_{r1} = K_{z1} = 10^{-4}$ ms^{-1}; $K_{r2} = K_{z2} = 10^{-6}$ ms^{-1}; $K_{r3} = K_{z3} = 10^{-6}$ ms^{-1}; $S_{s1} = 2\times10^{-5}$ m^{-1} ; $S_{s2} = 10^{-3}$ m^{-1} ; $S_{s3} = 10^{-6}$ m^{-1}; $Q_1 = 0.005$m^{3}s^{-1}; $Q = 0.002$m^{3}s^{-1}. One can see that the upper and lower unpumped layers have the same hydraulic properties of aquitard composed of clay soil for simplicity, and middle pumped layer may be composed of sand soils in reality. Under this circumstance, the three-layer system becomes a commonly investigated three-layer aquitard-aquifer-aquitard system (Hantush, 1960; Moench, 1985; Wen et al, 2011; Chen et al., 2020), which will be analyzed for comparison with existing works, though the presented solution applies to a general three-layer aquifer systems with no restrictions on the hydraulic parameter (e.g. permeability, specific storage) and the thickness of each layer. Aquifer anisotropy and different permeability contrasts among individual layers will also be explored to show the importance of considering both vertical and horizontal flows for each of the three layers, no matter the layer is pumped or unpumped.

3.1 Comparison with available solutions

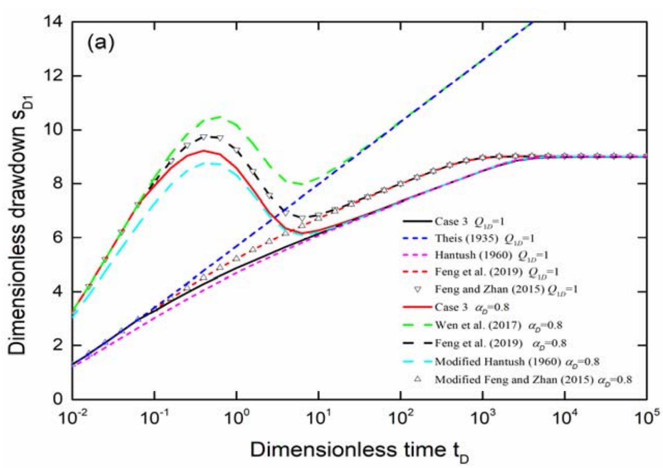

https://doi.org/10.5194/hess-2020-586
Preprint. Discussion started: 10 December 2020

Hydrology and Earth System Sciences
Discussions

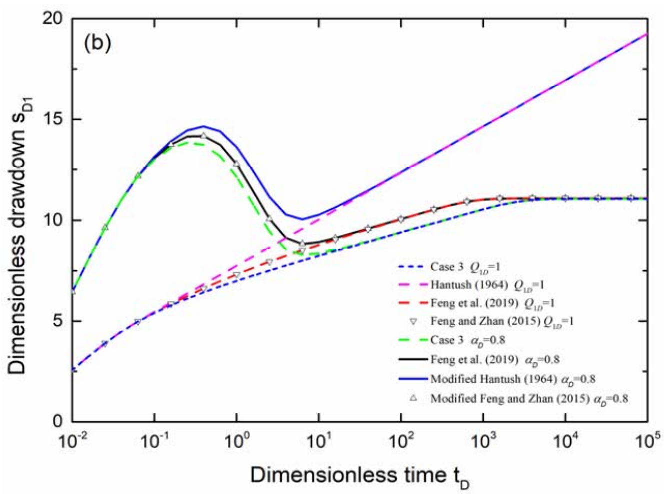

Fig.2 Comparison of the type curves for pumped layer provided by the newly developed solution for Case 3 and other existing solutions for a full penetration well (a) and a partial penetration well (b) with $r_D = 0.1$, $z_D = 0.5$, $\kappa_1 = \kappa_2 = 10^{-2}$, $\alpha_{Dz2} = \alpha_{Dr2} = 2 \times 10^{-4}$, $\alpha_{Dz3} = \alpha_{Dr3} = 2 \times 10^{-4}$, $\alpha_D = 0.8$, $Q_{1D} = 2.5$, $B_{D2} = 1.5$, $B_{D3} = 0.5$.

Fig. 2 (a) illustrates the drawdown responses of the pumped layer at $r_D = 0.1$ and $z_D = 0.5$ caused by a full penetration pumping well ($l_D = 1$, $d_D = 0$) in an aquitard-aquifer-aquitard system (Case 3 in this study, Hantush, 1960), an aquitard-aquifer system (Feng and Zhan, 2015, Feng et al. 2019), and a confined aquifer system (Theis, 1935, Wen et al., 2017). Fig. 2 (b) shows the pumped aquifer drawdown at the same location as Fig. 2 (a) due to a partial penetration pumping well ($l_D = 0.75$, $d_D = 0.25$) in present solution for Case 3, solutions of Feng and Zhan (2015) and Feng et al. (2019) for a leaky confined aquifer system, and Hantush (1964) for a nonleaky-confined aquifer system. Both the cases of constant ($Q_{1D} = 1$) and variable discharge ($Q_{1D} = 2.5$, $\alpha_D = 0.8$) are taken into account in this figure.

No matter what the well discharge is, under the circumstance of a full penetration well, the early-time drawdown for almost all study agree with one another except for the (modified)

https://doi.org/10.5194/hess-2020-586
Preprint. Discussion started: 10 December 2020

Hantush (1960) solution. The results are slightly larger than that of (modified) Hantush (1960) for an aquitard-aquifer-aquitard system if using the Hantush-Jacob approximation and the assumption of only considering the radial flow in the pumped layer and vertical flow in the unpumped aquitard. Because the leakage effect is regarded as a sink/source term introduced in the pumped aquifer governing equation in Hantush (1960), it is no strange to see a smaller drawdown in early time, as demonstrated in Fig. 2. The drawdown of Theis (1935) and Wen et al. (2017) with a full penetration well in Fig. 2 (a) or Hantush (1964) with a partial penetration well in Fig. 2 (b) is always larger than the others with the increasing of pumping time due to no leakage from adjacent layers. The intermediate time-drawdown in a leaky confined aquifer is greater than that in an aquitard-aquifer-aquitard system, which may be caused by less leakage into the pumped aquifer derived entirely from the upper aquitard storage. The late-time steady-state drawdowns can be found in two-layer and three-layer aquifer system and their values are almost the same as each other. Moreover, the time to approach the steady state for two-layer aquifer system (Feng and Zhan, 2015, Feng et al., 2019) is much earlier than that for three-layer aquifer system (Hantush, 1960, present study for Case 3), this is to be understood that the water from top boundary of the aquifer system of two-layer is also much quicker to supply the pumped aquifer because the pumped aquifer drawdown is not influenced by the storage of the lower layer in the aquifer system of three-layer.

Comparison of the dimensionless drawdown solution induced by a full penetration pumping well obtained by this study for Case 3 and (modified) Hantush (1960), one can only see the difference at early and intermediate times when t_D is smaller than about 10^2, as

https://doi.org/10.5194/hess-2020-586
Preprint. Discussion started: 10 December 2020

demonstrated in Fig. 2 (a). This can be attributed to the following aspects. Firstly, the Hantush-Jacob approximation is used in (modified) Hantush (1960). Secondly, the flow in the radial direction of aquitard and flow in the vertical direction of the pumped aquifer are not taken into consideration in (modified) Hantush (1960). However, the present study takes account of the horizontal and vertical flows in each layer, as we as treat the leakage across the two adjacent layers as continuity boundary conditions rather than a simplified volumetric sink/source term, accordingly, our general analytical model can reflect the actual leakage process. Therefore, one can conclude that the use of the Hantush-Jacob approximation should be deliberated, especially at the early pumping time for a fully penetrating well. One can see from Fig. 2 (b) that the storage of lower unpumped aquitard primarily affects the drawdown distribution for the three-layer aquifer system of Case 3 at the intermediate pumping time, signifying that the hydraulic parameters of lower aquitard can be estimated by using the observed data at this stage. In additional, more comparative analysis for the pumped aquifer drawdown in a confined aquifer with a pumping well of full penetration (Theis, 1935, Wen et al. (2017) or of partial penetration (Hautush, 1964) and in a two-layer aquifer with a full/partial penetration well (Feng and Zhan, 2015, Feng et al., 2019) can be found in the work of Feng et al. (2019), which is not repeated herein.

It should be remarked that the typical curves of drawdown versus pumping time have two inflection points during the decaying period of pumping rate, and more discussion and explanation for this feature can be found in Wen et al. (2017). At last, one can see from Fig. 2 (a) in comparison with Fig. 2 (b) that the pumped layer drawdown due to a partial penetration pumping well is greater than that a full penetration pumping well at the same value of

https://doi.org/10.5194/hess-2020-586
Preprint. Discussion started: 10 December 2020

pumping time, indicating that the effect of well partial penetration needs to be considered.

3.2 Effect of various top and bottom boundaries

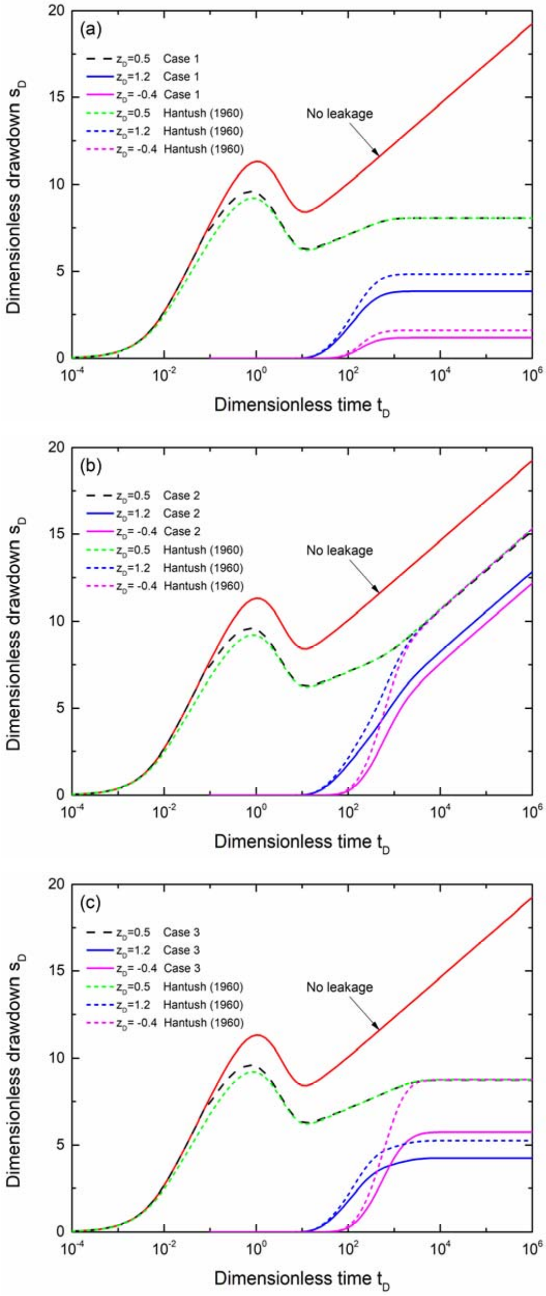

Fig.3 The typical curves of dimensionless drawdown versus dimension time in the pumped

https://doi.org/10.5194/hess-2020-586
Preprint. Discussion started: 10 December 2020

layer and unpumped layers under different top and bottom boundary (a) for Case1 (b) for Case 2 and (c) for Case 3 with $r_D = 0.1$, $z_D = 0.5$, $l_D = 1.0$, $d_D = 0$, $\kappa_1 = \kappa_2 = 10^{-2}$, $\alpha_{Dz2} = \alpha_{Dr2} = 2 \times 10^{-4}$, $\alpha_{Dz3} = \alpha_{Dr3} = 2 \times 10^{-4}$, $\alpha_D = 0.8$, $Q_{1D} = 2.5$, $B_{D2} = 1.5$, $B_{D3} = 0.5$.

Fig. 3 shows the changes of drawdown at $r_D = 0.1$ in the middle pumped layer ($z_D = 0.5$), in the upper layer ($z_D = 1.2$) and in the lower unpumped layer ($z_D = -0.4$) for Case 1 (a), Case 2 (b), and Case 3 (c) under the condition of a well of full penetration ($l_D = 1$, $d_D = 0$). The solution of Hantush (1960) is included in this figure for comparison purposes and the case of no leakage (Wen et al., 2017) is also considered as a reference. The curves of drawdown versus time for the pumped layer obtained by this study and Hantush (1960) have almost the same feature during the entire pumping stage and their deviations are mainly occurred at the stage of $10^{-2} < t_D < 10^1$, as illustrated in the subgraphs of Fig.3 with three different cases. Additionally, as for the drawdown response in the two unpumped layers, one can find from Fig.3 that the drawdown developed by this study is always larger than that of Hantush (1960) as the pumping time goes by and a relatively stable error between them can be found at late time. This is due to fact that the influence of radial flow in the unpumped layer is ignored by Hantush (1960). What is more, Fig. 3 (b) and Fig. 3 (c) demonstrate that the drawdown for the lower unpumped layer is nearly identical to that for the pumped layer if only taking account of the vertical flow in the unpumped layer. In other words, whether the radial flow in the unpumped layer is overlooked or not, one can see that from the comparison of drawdowns in the pumped layer with that in the unpumped layer for Case 2 and Case 3.

https://doi.org/10.5194/hess-2020-586
Preprint. Discussion started: 10 December 2020

Hydrology and Earth System Sciences
Open Access
Discussions

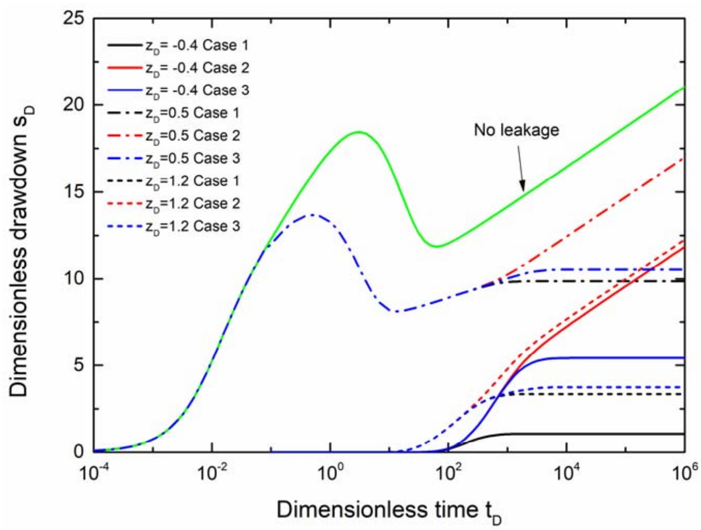

Fig.4 Comparison of the typical curves of dimensionless drawdown versus dimension time in the pumped layer and unpumped layers under diverse cases with $r_D = 0.1$, $z_D = 0.5$, $l_D = 0.75$, $d_D = 0.25$, $\kappa_1 = \kappa_2 = 10^{-2}$, $\alpha_{Dz2} = \alpha_{Dr2} = 2 \times 10^{-4}$, $\alpha_{Dz3} = \alpha_{Dr3} = 2 \times 10^{-4}$, $\alpha_D = 0.8$, $Q_{1D} = 2.5$, $B_{D2} = 1.5$, $B_{D3} = 0.5$.

In order to compare the drawdowns under different boundaries at the top and bottom of the aquifer system, Fig. 4 displays the drawdown changes at $r_D = 0.1$ in the pumped layer ($z_D = 0.5$) and in the unpumped layers ($z_D = 1.2$ and $z_D = -0.4$) for all three cases with a partial penetration pumping well ($l_D = 0.75$, $d_D = 0.25$). Notably, the no leaky case (modified, Hantush, 1964) is plotted as a reference in this figure. Fig. 4 shows that the influence of the type of top and boundary can be ignored in exploring drawdown at the early and intermediate pumping time, however, its influence on the late-time drawdown behavior is obvious, and one can find that the drawdowns for Cases 1 and 3 reach steady state at late pumping stage because of the unlimited water supply stemmed from the top zero-drawdown boundary. In addition, the late-time drawdown for Case 3 is greater than that for Case 1 and smaller than

https://doi.org/10.5194/hess-2020-586
Preprint. Discussion started: 10 December 2020

that for Case 2. This is due to the fact that the constant-head boundary at the top and bottom in Case 1 can give steady and unlimited supply of water, thus leading to the smallest drawdown among three cases. In another aspect, the no-flux top and bottom boundaries in Case 2 cannot furnish any supply of water, thus the largest drawdown can be seen among three cases in this figure.

Fig. 4 also illustrates that the drawdown for Case 2 increases indefinitely with pumping time and finally parallels with that of the no leakage case. This is caused by the no-flow boundary at the top and bottom. Furthermore, one cannot see the inflection point of the type curves for the unpumped layer, indicating that the influence of variable discharge mainly affects the pumped layer drawdown. This is because the drawdown response for the unpumped layer appears nearly at the end of the intermediate time and the influence of variable discharge is very small and can be neglected at this stage, thus the inflection point cannot be found.

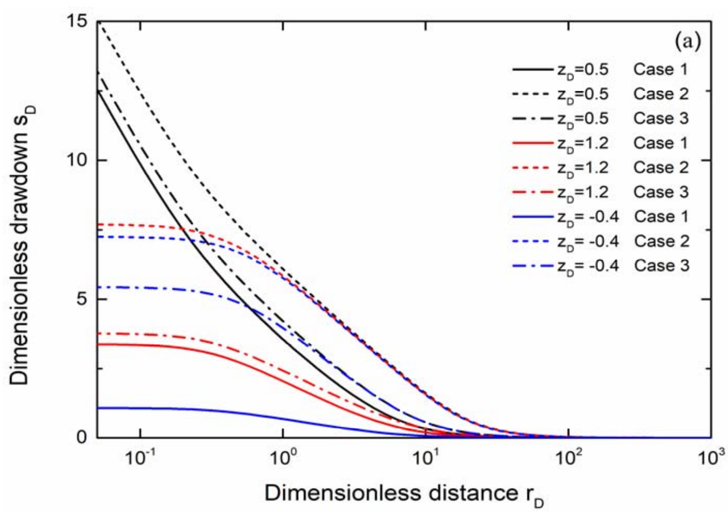

https://doi.org/10.5194/hess-2020-586
Preprint. Discussion started: 10 December 2020

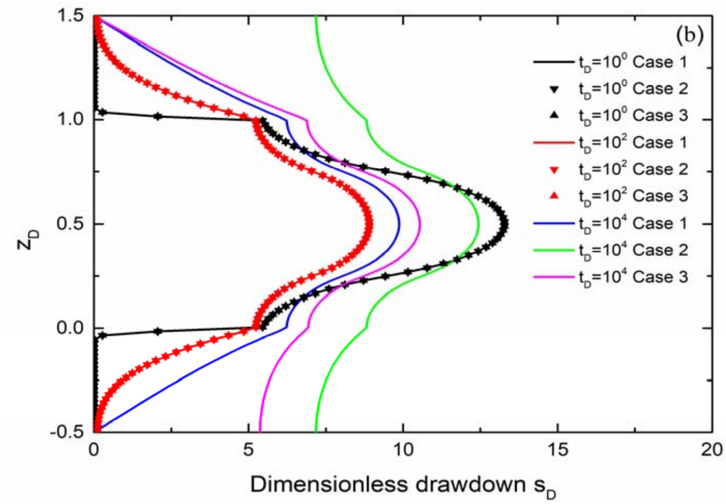

Fig.5 Comparison of the nondimensional drawdown behavior in the pumped layer and unpumped layers under diverse cases (a) the curves for s_D VS r_D at $t_D = 10^4$, (b) the curves for s_D VS z_D at $r_D = 0.1$with $l_D = 0.75$, $d_D = 0.25$, $\kappa_1 = \kappa_2 = 10^{-2}$, $\alpha_{Dz2} = \alpha_{Dr2} = 2 \times 10^{-4}$, $\alpha_{Dz3} = \alpha_{Dr3} = 2 \times 10^{-4}$, $\alpha_D = 0.8$, $Q_{1D} = 2.5$, $B_{D2} = 1.5$, $B_{D3} = 0.5$.

To further investigate the influence of various top and bottom boundaries on drawdown, Fig. 5 is plotted to demonstrate the drawdown responses in all layers using typical curves of (a) s_D versus r_D (z_D = 0.5, 1.2 and -0.4 at $t_D = 10^4$; (b) s_D versus z_D at $r_D = 0.1$ with a partial penetration pumping well ($l_D = 0.75$, $d_D = 0.25$). Fig. 5 (a) shows that the late-time drawdown at any radial distance r_D for Case 3 is greater than that for Case 1 and smaller than that for Case 2, and so does the pumping induced influence of the range for different cases, which is according with the above analysis of drawdown illustrated in Fig.4. It is interesting to find from Fig. 5 (a) that the drawdown in the pumped layer is nearly the same as that in the lower unpumped layer for Case 3 at $r_D > 10$, and the same phenomenon can be observed from Fig. 5 (a) for the drawdowns of Case 3 in the two unpumped layers and pumped layer for Case 3 if $r_D > 40$.

Additionally, the drawdowns along the vertical direction in whole aquifer system under various top and bottom boundaries are shown in Fig. 5 (b). To clarify, the pumping well of partial penetration is fixed in the middle of the pumped layer having a screen length of 0.5. It can be found that the drawdowns along the vertical direction for all three cases coincide with one another at early and intermediate pumping time (t_D = 1 and 10^2), however, the discrepancies among them are significant at a relatively late time of pumping ($t_D = 10^4$). An interesting observation from Fig. 5 (b) can be included that the drawdowns for Case 1 and Case 2 have symmetry with the axis $z_D = 0.5$ at the entire pumping time, which are caused by the identical top and bottom boundaries of the two cases and the same thickness and hydraulic parameters of the unpumped layers. However, the late-time drawdown for Case 3 has no symmetry and the lower layer drawdown is always smaller than that in the upper layer at correspondingly position of symmetry, this implies that the lower layer drawdown is influenced in a greater degree by pumping for Case 3. Besides, the largest drawdown at the axis of symmetry can be seen during the pumping period for all three cases, as expected. In general, one can conclude from Fig. 5 that the late-time drawdown is always affected by the type of top and bottom boundaries at any position within the three-layer aquifer system. Therefore, except for the location of piezometer (r and z), one had better clarify the types of top and bottom boundaries, if the late-time drawdown data are used for the estimation of parameters of the aquifer system of three-layer.

3.3 Effect of the variable pumping rate

Firstly, it points out that Case 3 is hereafter used as an example for demonstration purpose. It would be easy to analyze drawdown for Case 1 and Case 2 in a similar way when

https://doi.org/10.5194/hess-2020-586
Preprint. Discussion started: 10 December 2020

Hydrology and Earth System Sciences
Discussions

there is a need. One can know through the above analysis that the pumped aquifer drawdown is mainly influenced by the variable discharge. Fig. 6 shows only the pumped aquifer drawdown for Case 3 under different α_D at r_D = 0.1, 0.3 and 0.6. Note that $\alpha_D = \infty$ represents the final constant pumping rate. One can see that the differences among the type curves for different decay constants can be seen only at intermediate time. A greater α_D implies that the well discharge declines much faster to reach the final constant pumping rate, resulting in smaller drawdowns during the intermediate stage. Additionally, the inflection point of the curve of drawdown versus time near the pumping well is more obvious than that at a distance further away from the pumping well. This means that the effect of variable discharge decreases gradually with the increase of the radial distances and eventually disappears completely at some distances far enough. From previous study of Wen et al. (2017), one can use the point of inflection appeared at the stage of the declined pumping discharge at intermediate time to estimate aquifer parameters. Under this circumstances, Fig. 6 suggests that the observed data of drawdown near the pumping well would be a good choice.

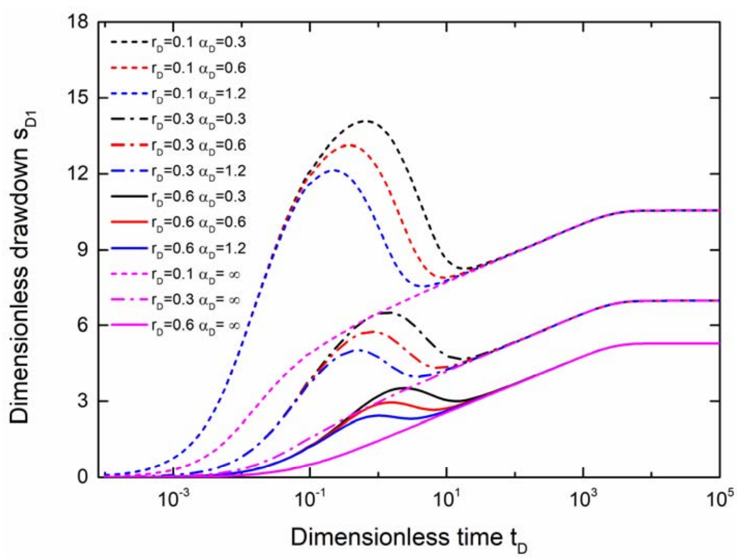

https://doi.org/10.5194/hess-2020-586
Preprint. Discussion started: 10 December 2020

Fig.6 Dimensionless drawdown response in the pumped layer and unpumped layers under different α_D for Case 3 with $z_D = 0.5$, $l_D = 0.75$, $d_D = 0.25$, $\kappa_1 = \kappa_2 = 10^{-2}$, $\alpha_{Dz2} = \alpha_{Dr2} = 2 \times 10^{-4}$, $\alpha_{Dz3} = \alpha_{Dr3} = 2 \times 10^{-4}$, $Q_{1D} = 2.5$, $B_{D2} = 1.5$, $B_{D3} = 0.5$.

3.4 Effect of the unpumped layer thickness

Fig. 7 shows the drawdown characteristics for the pumped ($z_D = 0.5$) and unpumped layer ($z_D = 1.1, -0.1$) at $r_D = 0.1$ with a partial penetration well ($l_D = 0.75$, $d_D = 0.25$) for various unpumped layer thickness ($B_D = B_{D3} = B_{D2} - 1$). Note that the no leakage case (or an impermeable unpumped layer) is also taken into consideration in this figure for comparison. The early and intermediate-drawdowns for both pumped aquifer and unpumped layers are not influenced by the change of the thickness of the unpumped layer, but the larger the thickness of the unpumped layer, the larger late-time drawdown can be found. In addition, Fig. 7 also illustrates that the pumped aquifer drawdown is significantly influenced by the leakage from adjacent layer if compared to the case of no leakage.

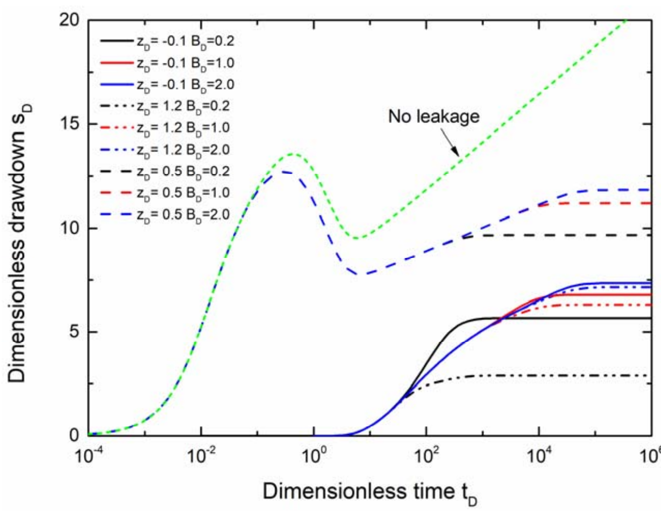

Fig.7 Dimensionless drawdown response in the pumped layer and unpumped layers under

https://doi.org/10.5194/hess-2020-586
Preprint. Discussion started: 10 December 2020

different thickness of the unpumped layers ($B_D = B_{D2} - 1 = B_{D3}$) for Case 3 with $r_D = 0.1$, $z_D = 0.5$, $l_D = 0.75$, $d_D = 0.25$, $\kappa_1 = \kappa_2 = 10^{-2}$, $\alpha_{Dz2} = \alpha_{Dr2} = 2 \times 10^{-4}$, $\alpha_{Dz3} = \alpha_{Dr3} = 2 \times 10^{-4}$, $\alpha_D = 0.8$, $Q_{1D} = 2.5$, $B_{D2} = 1.5$, $B_{D3} = 0.5$.

3.5 Effect of anisotropy

Because of the generality of the established solution, one can easily explore the influence of anisotropy for each layer on the drawdown in this three-layer system. To be sure, two schemes of the aquifer system are considered for comparison. The drawdown change in the classical aquitard-aquifer-aquitard scheme (termed scheme A herein) will show in the following figures (a), and the drawdown response will also be illustrated in the following figures (b) for another scheme (termed scheme B herein) of a general aquifer system of three-layer, having the permeability values of the upper and lower layers being one order of magnitude smaller (instead of two orders of magnitude smaller as in the default setting) than that of the middle-pumped layer.

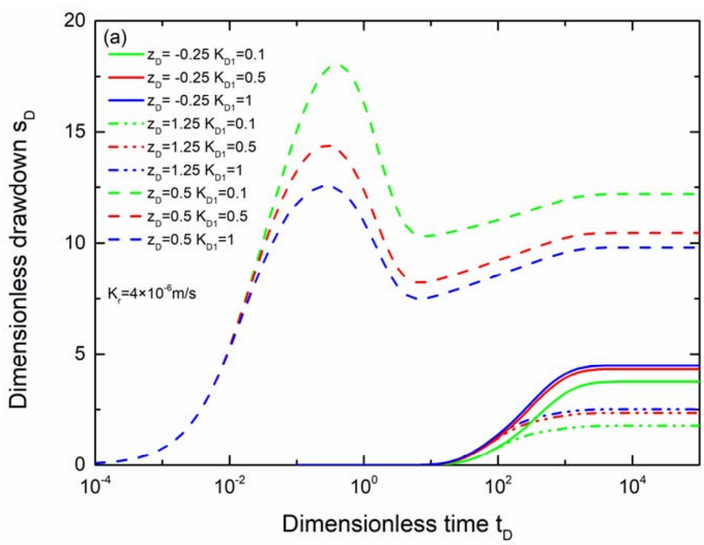

https://doi.org/10.5194/hess-2020-586
Preprint. Discussion started: 10 December 2020

Hydrology and Earth System Sciences
Discussions

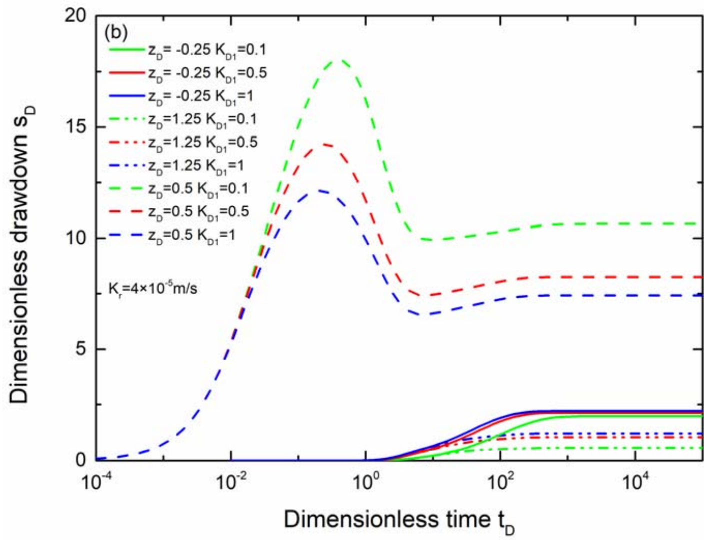

Fig.8 The nondimensional drawdown response in the pumped layer and unpumped layers under different anisotropy of the pumped layer ($K_{D1} = K_{z1}/K_{r1}$) for Case 3 with $r_D = 0.1$, $\alpha_D = 0.8$, $Q_{1D} = 2.5$, $B_{D2} = 1.5$, $B_{D3} = 0.5$, $l_D = 0.75$, $d_D = 0.25$, $K_{D2} = K_{z2}/K_{r2} = K_{D3} = K_{z3}/K_{r3} = 0.2$, where (a) $K_r = K_{r2} = K_{r3} = 4\times10^{-6}$m/s, (b) $K_r = K_{r2} = K_{r3} = 4\times10^{-5}$m/s.

Fig. 8 shows the response of drawdown for Case 3 in the pumped layer ($z_D = 0.5$) and in the upper and lower layers ($z_D = 1.25$, -0.25) at $r_D = 0.1$ with a partial penetration well ($l_D = 0.75$, $d_D = 0.25$) for various anisotropy of the pumped layer ($K_{D1} = K_{z1}/K_{r1}$). Note that $K_{D1} = 1$ refers to the isotropic case, which is included as a reference.

One can see from Fig. 8 that the entire aquifer system for scheme A and scheme B is affected by the change of the pumped layer anisotropy almost during the entire pumping time. The pumped layer drawdown decreases with an increase of the anisotropy ratio and a larger K_{D1} results in larger drawdowns for the upper and lower unpumped layers. Comparing the drawdowns for scheme A shown in Fig. 8 (a) and for scheme B listed in Fig. 8 (b), one can see that the drawdown for scheme A is always larger than that for scheme B. This is because

https://doi.org/10.5194/hess-2020-586
Preprint. Discussion started: 10 December 2020

Hydrology and Earth System Sciences
Open Access
Discussions

the difference of the permeability of the unpumped layers and pumped layer for scheme B is not as significant as that for scheme A, and the capacity of water supply of the unpumped layers for scheme B is much stronger than that for scheme A. Therefore, it is much easier to obtain the water supply from the top boundary, thus a smaller drawdown is seen as illustrated in Fig. 8 (b). Overall, the pumped layer anisotropy is of great importance to ascertaining the drawdown behavior of the entire three-layer aquifer system.

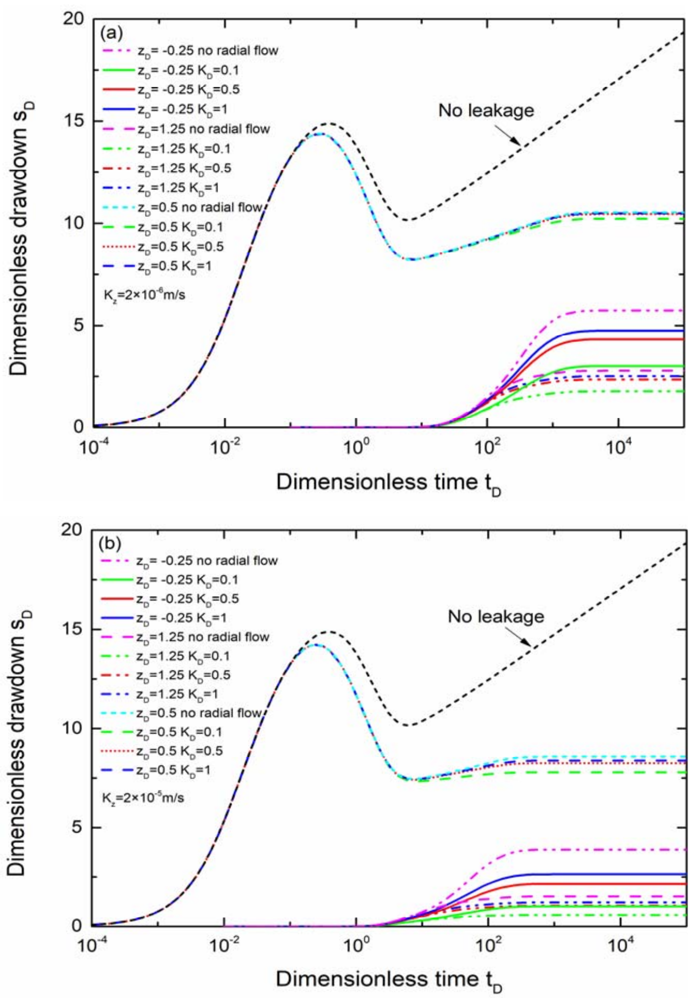

Fig.9 The nondimensional drawdown change in the pumped layer and unpumped layers under different anisotropy of the unpumped layers ($K_D = K_{z2}/K_{r2} = K_{z3}/K_{r3}$) for Case 3 with

https://doi.org/10.5194/hess-2020-586
Preprint. Discussion started: 10 December 2020

Hydrology and Earth System Sciences
Discussions

$r_D = 0.1$, $\alpha_{Dz2} = \alpha_{Dz3} = 2 \times 10^{-4}$, $\alpha_D = 0.8$, $Q_{1D} = 2.5$, $B_{D2} = 1.5$, $B_{D3} = 0.5$, $K_{D1} = K_{z1}/K_{r1} = 0.5$, $K_{r2} = K_{r3}$, $l_D = 0.75$, $d_D = 0.25$, in which (a) $\kappa_1 = \kappa_2 = 0.04$, $\alpha_{Dr2} = \alpha_{Dr3} = 4 \times 10^{-5}$, $K_z = K_{z2} = K_{z3} = 2\times10^{-6}$m/s and (b) $\kappa_1 = \kappa_2 = 0.4$, $\alpha_{Dr2} = \alpha_{Dr3} = 4 \times 10^{-4}$, $K_z = K_{z2} = K_{z3} = 2\times10^{-5}$m/s.

Fig. 9 demonstrates the drawdown changes for Case 3 in an anisotropic pumped layer ($z_D = 0.5$, $K_{D1} = 0.5$ and $K_{r1} = 10^{-4}\ m/s$) and anisotropic upper and lower layers ($z_D = 1.25$ and -0.25) for various anisotropy ratios of unpumped layer ($K_D = K_{D2} = K_{z2} / K_{r2} = K_{D3} = K_{z3} / K_{r3}$) at $r_D = 0.1$ with a pumping well of partial penetration ($l_D = 0.75$ and $d_D = 0.25$). It should be mentioned that the vertical permeability of the unpumped layer is to be kept on hold in Fig. 9, where (a) $K_z = K_{z2} = K_{z3} = 2\times10^{-6} m/s$ and (b) $K_z = K_{z2} = K_{z3} = 2\times10^{-5}$m/s. The case of an isotropic unpumped layer ($K_D = 1$) is considered in both subgraphs, and the case of ignoring the radial flow in unpumped layer is depicted as well for comparison in Fig. 9. One can obviously see from Fig. 9 that the influence of various anisotropy ratios on the pumped layer drawdowns almost coincide with the case of the unpumped layer with no horizontal low for scheme A if $K_D \geq 0.5$. However, when K_D is 0.1 for scheme A, the anisotropy of the unpumped layers significantly affects the pumped layer drawdown at the late pumping time as demonstrated in Fig. 9 (a). The influence of the unpumped layers anisotropy on the pumped layer drawdown for scheme B is more obvious than that for scheme A at intermediate and late times, it can be seen from Fig. 9 (b). In addition, no matter what the value of anisotropy K_D is, the change of K_D has an appreciable influence on the unpumped layer drawdowns for both scheme A and scheme B. Finally, one still can conclude from Fig. 9 that the drawdown for scheme A is generally larger than that for scheme B at the same position within the aquifer system of three-layer and at the same pumping time. Overall, the

https://doi.org/10.5194/hess-2020-586
Preprint. Discussion started: 10 December 2020

Hydrology and Earth System Sciences
Discussions

radial and vertical flows in the unpumped layer (effect of anisotropy) should be considered in determining drawdown responses around the pumping well, especially to the general case without large contrast of hydraulic conductivity among the unpumped layers and the pumped layer.

3.6 The effect of well partial penetration

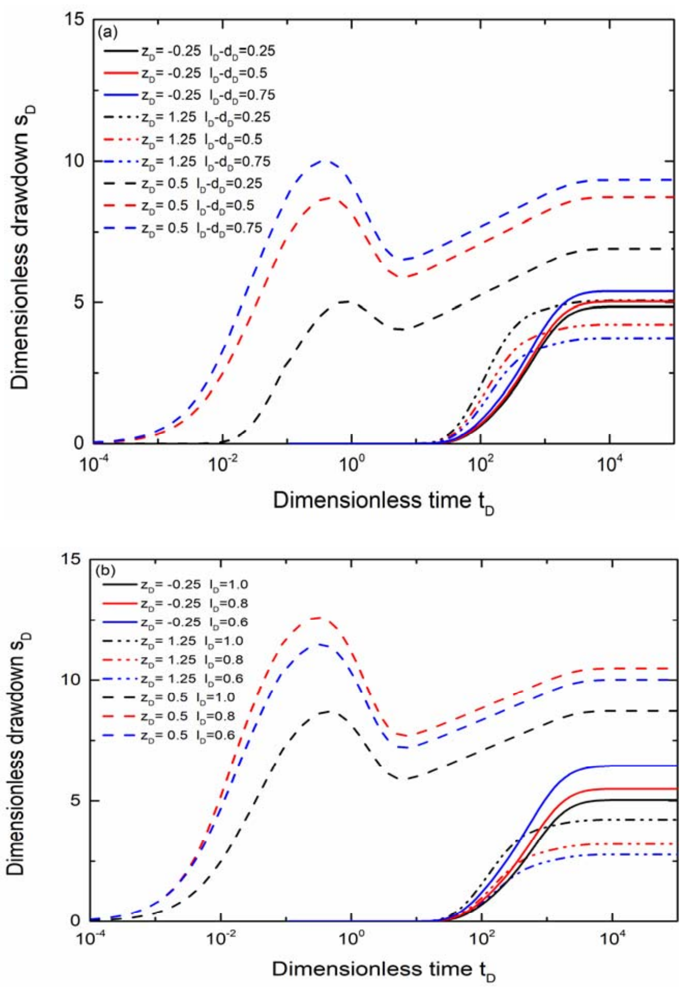

Fig. 10 Drawdown responses in the pumped layer and unpumped layers (Case 3) with r_D = 0.1, $\kappa_1 = \kappa_2 = 10^{-2}$, $\alpha_{Dz2} = \alpha_{Dr2} = 2 \times 10^{-4}$, $\alpha_{Dz3} = \alpha_{Dr3} = 2 \times 10^{-4}$, $\alpha_D = 0.8$, $Q_{1D} = 2.5$, $B_{D2} = 1.5$, $B_{D3} = 0.5$ (a) for different well screen length, in which $l_D = 1.0$ (b) for various depth of well

https://doi.org/10.5194/hess-2020-586
Preprint. Discussion started: 10 December 2020

screen within the middle pumped layer, where l_D - d_D = 0.5.

One of the main contributions in this study is that the established general analytical model considered the effect of the well partial penetration, Fig. 10 shows the drawdown changes for Case 3 (r_D = 0.1) in the middle-pumped layer (z_D = 0.5) and unpumped layers (z_D = 1.25 and -0.25). Especially, Fig. 10 (a) is for various well screen length and l_D = 1.0, and Fig. 10 (b) is for different vertical position of well screen within the middle-pumped layer and the well screen length is fixed (l_D - d_D = 0.5). It can be seen from Fig. 10 that the length and position of well screen have remarkable effect on the drawdown for all three layers. A larger well screen length means that the middle drawdown of pumped layer is closer to the position of well screen and the stored water is much easier to be released, resulting in a larger drawdown of pumped layer, similarly, a smaller drawdown for the upper layer and a greater drawdown for the lower unpumped layer can be seen in Fig. 10 (a) for Case 3. Additionally, one can conclude from the above analysis shown in Fig. 5 (b) that the closer to the center of the pumped well, the larger drawdown can be seen for all three layers, and the drawdown for the lower layer is relatively larger than the late-time drawdown for the upper layer at the same distance measured from the interface between the pumped layer and unpumped layer for Case 3. The center point of the well screen for three different l_D = 1.0, 0.8 and 0.6 is respectively at z_D = 0.75, 0.55 and 0.35, respectively. Thus, the pumped layer drawdown (z_D = 0. 5) with l_D = 0.6 is larger than that with l_D = 1.0 and smaller than that with l_D = 0.8, in the same way, the upper unpumped layer drawdown (z_D = 1.25) with l_D = 0.8 is larger than that with l_D = 0.6 and smaller than that with l_D = 1.0, and the lower unpumped layer drawdown

https://doi.org/10.5194/hess-2020-586
Preprint. Discussion started: 10 December 2020

Hydrology and Earth System Sciences
Open Access
EGU
Discussions

(z_D = -0.25) with l_D = 0.8 is larger than that with l_D = 1.0 and smaller than that with l_D = 0.6. Besides that, whatever the pumping well is located at the pumped layer, the pumping induced drawdown in the lower unpumped layer is larger than that in the upper layer for Case 3.

4. Discussion

Based upon the presented solution, firstly, one can perform quantitative evaluation of the dimensionless drawdown at any points within the general three-layer aquifer system with a partial penetration pumping well in the middle layer. It is worth emphasizing again that the developed solution not only has no any restrictions on the values of the thickness, hydraulic conductivity, and specific storage for all three layers, but that for the length and location of the well screen fixed in the pumped layer, thus, the generality of the obtained solution is the main contribution of this study. Secondly, it is convenient to explore the influences of variable discharge of pumping, aquifer thickness, anisotropy, well partial penetration, and the type of top and bottom boundary on the groundwater flow problems in the aquifer system of three-layer. Besides that, the present solutions have a powerful potentiality within geotechnical engineering, petroleum engineering and groundwater resource development. Another important application of the proposed solution is to identify the hydraulic parameters of each layer with adopting the method of parameter estimation in conjunction with field data.

Because the responses for a special case of aquitard-aquifer-aquifer system is mainly explored for comparison with existing solutions, some suggestions can be obtained for using the developed solutions in such a three-layer aquifer from the above analysis herein. First of all, the well structure (screen position and length) in the pumped layer and the thickness of all

https://doi.org/10.5194/hess-2020-586
Preprint. Discussion started: 10 December 2020

Hydrology and Earth System Sciences Discussions
Open Access

layers should be clearly determined. Secondly, the type of boundary at the top and bottom of the aquifer system should be clarified with the use of the observed data of late-time drawdown for parameter estimation. Thirdly, the feature of inflection point for the curve of drawdown against time due to the effect of variable discharge can be used to estimate the pumped layer parameters, and in such a case the *in situ* data of drawdown in vicinity of the pumping well need to be collected. Fourthly, the data of early-time drawdown for unpumped layers are suggested to determine their specific storage respectively, the datum of late-time drawdown for unpumped layers can be applied to estimate their values of hydraulic conductivities respectively.

However, a few limitations of this study are also need to be addressed. Firstly, the effects of finite radius and wellbore storage on flow cannot be investigated in this study because of the assumption of infinitesimal radius of the pumping well. Secondly, the three-dimensional transient responses in three-layer aquifer system have not been discussed with the condition of constant-drawdown pumping, other type of variable-rate pumping (e.g. sinusoidal pumping, piecewise-linear pumping), etc. Thirdly, the heterogeneity of the aquifer and varying/non-uniform thickness of each layer are not taken into consideration. Fourthly, the slope of each layer and the influence of finite or non-uniform well skin are not considered as well. Fifthly, the effect of a finite or irregular lateral boundary is not analyzed. The investigation for these subjects is much needed in details in the future.

5. Summary and conclusions

A general semi-analytical dimensionless drawdown solution in an anisotropic aquifer system of three-layer caused by a partial penetration well pumped at a variable discharge is

https://doi.org/10.5194/hess-2020-586
Preprint. Discussion started: 10 December 2020

Hydrology and Earth System Sciences
Discussions

developed by means of Laplace-Hankel transformation taking account of the interface flow. Most importantly, three widely used types of boundary conditions at the top and bottom are considered that include a zero-drawdown boundary for Case1 or a no-flow boundary for Case 2, and a constant-head boundary at the top in combination with a no-flux boundary at the bottom for Case 3. The time-domain solutions are evaluated by performing numerical inversion of the transformations of Laplace and Hankel. The present solutions encompass some previously known solutions caused by a full or partial penetration pumping well in an aquifer system of two-layer or single-layer as subsets. The three-dimensional transient drawdown in the entire aquifer system pumped by a partial penetration well having a discharge with exponentially decaying function in the middle layer is explored as an example of illustration. From this study, one can conclude the following main findings:

(1) The pumped layer drawdown for Hantush (1960) with neglecting vertical flow in the pumped layer and horizontal flow in the unpumped layer and the use of the Hantush-Jacob approximation is greater that of this work for Case 2, especially at the early pumping time for a fully penetrating well, and the unpumped layers drawdown for Hantush (1960) are greater than that for present study.

(2) The effect of variable discharge describing an exponential decline function of pumping time mainly affects the drawdown of the pumped layer, and a noticeable feature of inflection points can be seen at the stage of the decay of well discharge and the region nearby the well of pumping.

(3) The type of boundary at the top and bottom of the aquifer system has no influence on the early- and intermediate-drawdown, but the drawdown at late pumping time for Case 3 is

Hydrology and Earth System Sciences
Open Access
EGU
Discussions

greater than that for Case 1 and smaller than that for Case 2 in all three layers.

(4) A smaller anisotropy ratio (meaning a smaller vertical/horizontal permeability ratio) of the pumped layer results in a larger pumped layer drawdown and a smaller unpumped layer drawdown over the whole pumping times. The anisotropy of the unpumped layers (K_D) mainly affects the drawdown in the unpumped layer and a larger anisotropy ratio (K_D) leads to a larger drawdown of unpumped layer.

(5) The anisotropy of the unpumped layers significantly affects the drawdown in the aquifer system without large contrast of hydraulic conductivity between the unpumped layers and the pumped layer during entire pumping period.

(6) The drawdown nearby the pumping well in all three layers are significantly affected by the length and position of well screen in the pumped layer at the entire time, and a larger drawdown can be seen at the position of a smaller distance to the midpoint of the well screen.

Author contributions. F.QG., and F.XL., conceived the presented idea, F.QG., developed the solutions and codes for the model, F.QG., and Z.HB., performed the results and discussion. F.XL., and Z.HB., supervised the findings of the study. All authors contributed to the writing and the final paper.

Competing interest. The authors declare that they have no conflict of interest.

Acknowledgements. This research was partially funded by the National Natural Science Foundation of China (No. 41702336) and the research project for Wuhan Municipal Construction Group Co., Ltd. (No. wszky201820).

https://doi.org/10.5194/hess-2020-586
Preprint. Discussion started: 10 December 2020

Hydrology and Earth System Sciences
Discussions

Appendix A. Derivations of solutions for different cases

The Laplace and Hankel transformation technique are sequentially applied to Eqs. (17) – (33), one can obtain the following Laplace-Hankel domain governing equations of flow in the middle-pumped aquifer

$$\frac{\partial^2 \hat{\bar{s}}_{D1}}{\partial z_D^2} - \xi_1 \hat{\bar{s}}_{D1} = \frac{1}{\alpha_{Dz1}} \lim_{r_D \to 0} r_D \frac{\partial^2 \bar{s}_{D1}}{\partial r_D} \quad \text{(A1)}$$

with

$$\lim_{r \to 0} r_D \frac{\partial \bar{s}_{D1}}{\partial r_D} = \begin{cases} 0 & l_D < z_D \le 1 \\ -\dfrac{2\bar{Q}(p)}{l_D - d_D} & d_D \le z_D \le l_D \\ 0 & 0 \le z_D < d_D \end{cases} \quad \text{(A2)}$$

and the variable discharge used in this study is expressed in Eq. (5), one can obtain,

$$\bar{Q}(p) = \frac{1}{p} + \frac{Q_{1D} - 1}{p + \alpha_D} \quad \text{(A3)}$$

Substituting Eq. (A3) into Eq. (A2) results in

$$\lim_{r_D \to 0} r_D \frac{\partial \bar{s}_{D1}}{\partial r_D} = \begin{cases} 0 & l_D < z_D \le 1 \\ -\dfrac{2}{l_D - d_D}\left(\dfrac{1}{p} + \dfrac{Q_{1D} - 1}{p + \alpha_D}\right) & d_D \le z_D \le l_D \\ 0 & 0 \le z_D < d_D \end{cases} \quad \text{(A4)}$$

To derive the solution of Eq. (A1), using the method proposed by Neuman (1974), the dimensionless drawdown for the middle-pumped layer (s_{D1}) can be divided into the following form and written in Laplace-Hankel space as:

$$\hat{\bar{s}}_{D1} = \hat{\bar{u}}_D + \hat{\bar{v}}_D \quad \text{(A5)}$$

in which $\hat{\bar{u}}_D$ designates the Laplace-Hankel domain drawdown solution in a confined aquifer caused by a partial penetration pumping well, and the final expression of $\hat{\bar{u}}_D$ written in Eq. (33) can be obtained by complying with the analogous process adopted by Feng and Zhan (2019). $\hat{\bar{v}}_D$ satisfies Eqs. (17) and (24)-(27).

https://doi.org/10.5194/hess-2020-586
Preprint. Discussion started: 10 December 2020

Hydrology and Earth System Sciences
Open Access
Discussions

Under this circumstance, the governing equation of $\hat{\bar{v}}_D$ becomes

$$\frac{\partial^2 \hat{\bar{v}}_D(\lambda, z_D, p)}{\partial z_D^2} - \xi_1^2 \hat{\bar{v}}_D(\lambda, z_D, p) = 0 \qquad \text{(A6)}$$

By analogy, the governing equations of the upper and lower unpumped layer are respectively rewritten as

$$\frac{\partial^2 \hat{\bar{s}}_{D2}(\lambda, z_D, p)}{\partial z_D^2} - \xi_2^2 \hat{\bar{s}}_{D2}(\lambda, z_D, p) = 0 \qquad \text{(A7)}$$

and

$$\frac{\partial^2 \hat{\bar{s}}_{D3}(\lambda, z_D, p)}{\partial z_D^2} - \xi_3^2 \hat{\bar{s}}_{D3}(\lambda, z_D, p) = 0 \qquad \text{(A8)}$$

The interface boundary conditions at $z_D = 1$ given in Eqs. (24) and (25) become

$$\hat{\bar{u}}_D(\lambda, 1, p) + \hat{\bar{v}}_D(\lambda, 1, p) = \hat{\bar{s}}_{D2}(\lambda, 1, p), \qquad z_D = 1 \qquad \text{(A10)}$$

$$\frac{\partial \hat{\bar{v}}_D(\lambda, z_D, p)}{\partial z_D} = \kappa_1 \frac{\partial \hat{\bar{s}}_{D2}(\lambda, z_D, p)}{\partial z_D}, \qquad z_D = 1 \qquad \text{(A11)}$$

And considering the boundary conditions at $z_D = 0$ expressed in Eqs. (26) and (27), one can obtain

$$\hat{\bar{u}}_D(\lambda, z_D, p) + \hat{\bar{v}}_D(\lambda, z_D, p) = \hat{\bar{s}}_{D3}(\lambda, z_D, p), \qquad z_D = 0 \qquad \text{(A12)}$$

$$\frac{\partial \hat{\bar{v}}_D(r_D, z_D, p)}{\partial z_D} = \kappa_2 \frac{\partial \hat{\bar{s}}_{D3}(r_D, z_D, p)}{\partial z_D}, \qquad z_D = 0 \qquad \text{(A13)}$$

Finally, the top and bottom boundary conditions given in Eqs. (28)-(33) can be rewritten as:

For Case 1,

$$\hat{\bar{s}}_{D2}(r_D, z_D, p) = 0, \quad z_D = B_{D2} \qquad \text{(A14)}$$

$$\hat{\bar{s}}_{D3}(r_D, z_D, p) = 0, \quad z = -B_{D3} \qquad \text{(A15)}$$

For Case 2,

https://doi.org/10.5194/hess-2020-586
Preprint. Discussion started: 10 December 2020

Hydrology and Earth System Sciences
Open Access
EGU
Discussions

$$\frac{\partial \hat{\bar{s}}_{D2}\left(r_D, z_D, p\right)}{\partial z} = 0, \quad z_D = B_{D2} \qquad \text{(A16)}$$

$$\frac{\partial \hat{\bar{s}}_{D3}\left(r_D, z_D, p\right)}{\partial z_D} = 0, \quad z_D = -B_{D3} \qquad \text{(A17)}$$

and

for Case 3,

$$\hat{\bar{s}}_{D2}\left(r_D, z_D, p\right) = 0, \quad z_D = B_{D2} \qquad \text{(A18)}$$

$$\frac{\partial \hat{\bar{s}}_{D3}\left(r_D, z_D, p\right)}{\partial z_D} = 0, \quad z_D = -B_{D3} \qquad \text{(A19)}$$

The general solution for Eq. (A6) is

$$\hat{\bar{v}}_D\left(\lambda, z_D, p\right) = c_1 e^{\xi_1 z_D} + c_2 e^{-\xi_1 z_D} \qquad \text{(A20)}$$

Substituting Eq. (A20) into Eq. (A5), one can write

$$\hat{\bar{s}}_{D1} = \hat{\bar{u}}_D\left(\lambda, z_D, p\right) + c_1 e^{\xi_1 z_D} + c_2 e^{-\xi_1 z_D} \qquad \text{(A21)}$$

The general solutions of Eqs. (A7) and (A8) for flow in the upper and lower unpumped layers can be expressed, respectively, as

$$\hat{\bar{s}}_{D2} = c_3 e^{\xi_2 z_D} + c_4 e^{-\xi_2 z_D} \qquad \text{(A22)}$$

and

$$\hat{\bar{s}}_{D3} = c_5 e^{\xi_3 z_D} + c_6 e^{-\xi_3 z_D} \qquad \text{(A23)}$$

Using the continuity boundary conditions of Eqs. (A10)-(A13) leads to

$$\hat{\bar{u}}_D\left(\lambda, 1, p\right) + c_1 e^{\xi_1} + c_2 e^{-\xi_1} - c_3 e^{\xi_2} - c_4 e^{-\xi_2} = 0 \qquad \text{(A24)}$$

$$c_1 e^{\xi_1} - c_2 e^{-\xi_1} - \gamma_1\left(c_3 e^{\xi_2} - c_4 e^{-\xi_2}\right) = 0 \qquad \text{(A25)}$$

$$\hat{\bar{u}}_D\left(\lambda, 0, p\right) + c_1 + c_2 - c_5 - c_6 = 0 \qquad \text{(A26)}$$

and

$$c_1 - c_2 - \gamma_2\left(c_5 - c_6\right) = 0 \qquad \text{(A27)}$$

https://doi.org/10.5194/hess-2020-586
Preprint. Discussion started: 10 December 2020

Hydrology and Earth System Sciences Discussions
Open Access

Applying the top and bottom boundary conditions Eqs. (A10)-(A13), one can write

Case 1,

$$c_3 e^{\xi_2 B_{D2}} + c_4 e^{-\xi_2 B_{D2}} = 0 \quad \text{(A28)}$$

$$c_5 e^{-\xi_3 B_{D3}} + c_6 e^{\xi_3 B_{D3}} = 0 \quad \text{(A29)}$$

Case 2,

$$c_3 e^{\xi_2 B_{D2}} - c_4 e^{-\xi_2 B_{D2}} = 0 \quad \text{(A30)}$$

$$c_5 e^{-\xi_3 B_{D3}} - c_6 e^{\xi_3 B_{D3}} = 0 \quad \text{(A31)}$$

and

Case 3,

$$c_3 e^{\xi_2 B_{D2}} + c_4 e^{-\xi_2 B_{D2}} = 0 \quad \text{(A32)}$$

$$c_5 e^{-\xi_3 B_{D3}} - c_6 e^{\xi_3 B_{D3}} = 0 \quad \text{(A33)}$$

Solving equations consisting of expressions (A24)–(A27) and (A28)–(A29), the coefficients that need to be determined for Case 1 are

$$c_1 = \frac{2}{\chi_1}\left\{\begin{array}{l}\hat{\bar{u}}\left(r_D,0,p\right)e^{-\xi_1}\gamma_2\left[\left(\cosh\theta_1+\cosh\theta_2\right)\gamma_1-\left(\sinh\theta_1+\sinh\theta_2\right)\right]\\ -\hat{\bar{u}}\left(r_D,1,p\right)\gamma_1\left[\left(\cosh\theta_1+\cosh\theta_2\right)\gamma_2+\sinh\theta_1-\sinh\theta_2\right]\end{array}\right\} \quad \text{(A34a)}$$

and

$$c_2 = -\frac{2}{\chi_1}\left\{\begin{array}{l}2\hat{\bar{u}}\left(r_D,0,p\right)e^{\xi_1}\gamma_2\left[\left(\cosh\theta_1+\cosh\theta_2\right)\gamma_1+\sinh\theta_1+\sinh\theta_2\right]\\ -2\hat{\bar{u}}\left(r_D,1,p\right)\gamma_1\left[\left(\cosh\theta_1+\cosh\theta_2\right)\gamma_2-\left(\sinh\theta_1-\sinh\theta_2\right)\right]\end{array}\right\} \quad \text{(A34b)}$$

with c_3, c_4, c_5, and c_6 written by c_1 and c_2.

$$c_3 = \frac{1}{2\gamma_1}e^{-\xi_2}\left[c_1 e^{\xi_1}\left(\gamma_1+1\right)+c_2 e^{-\xi_1}\left(\gamma_1-1\right)+\gamma_1\hat{\bar{u}}_D\left(r_D,1,p\right)\right] \quad \text{(A34c)}$$

$$c_4 = \frac{1}{2\gamma_1}e^{-\xi_2}\left[c_1 e^{\xi_1}\left(\gamma_1-1\right)+c_2 e^{-\xi_1}\left(\gamma_1+1\right)+\gamma_1\hat{\bar{u}}_D\left(r_D,1,p\right)\right] \quad \text{(A34d)}$$

$$c_5 = \frac{1}{2\gamma_2}\left[c_1\left(\gamma_2+1\right)+c_2\left(\gamma_2-1\right)+\gamma_2\hat{\bar{u}}_D\left(r_D,0,p\right)\right] \quad \text{(A34e)}$$

$$c_6 = \frac{1}{2\gamma_2}\left[c_1\left(\gamma_2-1\right)+c_2\left(\gamma_2+1\right)+\gamma_2\hat{\bar{u}}_D\left(r_D,0,p\right)\right] \quad \text{(A34f)}$$

where

https://doi.org/10.5194/hess-2020-586
Preprint. Discussion started: 10 December 2020

Hydrology and Earth System Sciences
Open Access
Discussions

$$\begin{aligned}\chi_1 = {} & 2(1+\gamma_1)(1+\gamma_2)\sinh(\xi_1+\theta_1) + 2(1-\gamma_1)(1-\gamma_2)\sinh(\xi_1-\theta_1) \\ & -2(1+\gamma_1)(1-\gamma_2)\sinh(\xi_1+\theta_2) - 2(1-\gamma_1)(1+\gamma_2)\sinh(\xi_1-\theta_2)\end{aligned} \quad \text{(A34g)}$$

Similarly, solving equations including Eqs. (A20)–(A24) and Eqs. (A28)–(A29), the related coefficients used in Case 2 yield

$$c_1 = \frac{2}{\chi_2}\left\{\begin{aligned} & \hat{\bar{u}}(r_D,0,p)e^{-\xi_1}\gamma_2\left[(\cosh\theta_2-\cosh\theta_1)\gamma_1+(\sinh\theta_1-\sinh\theta_2)\right] \\ & +\hat{\bar{u}}(r_D,1,p)\gamma_1\left[(\cosh\theta_1-\cosh\theta_2)\gamma_2+(\sinh\theta_1+\sinh\theta_2)\right]\end{aligned}\right\} \quad \text{(A35a)}$$

$$c_2 = -\frac{2}{\chi_2}\left\{\begin{aligned} & \hat{\bar{u}}(r_D,0,p)e^{\xi_1}\gamma_2\left[(\cosh\theta_2-\cosh\theta_1)\gamma_1-(\sinh\theta_1-\sinh\theta_2)\right] \\ & +\hat{\bar{u}}(r_D,1,p)\gamma_1\left[(\cosh\theta_1-\cosh\theta_2)\gamma_2-(\sinh\theta_1+\sinh\theta_2)\right]\end{aligned}\right\} \quad \text{(A35b)}$$

$$c_3 = \frac{1}{2\gamma_1}e^{-\xi_2}\left[c_1e^{\xi_1}(\gamma_1+1)+c_2e^{-\xi_1}(\gamma_1-1)+\gamma_1\hat{\bar{u}}_D(r_D,1,p)\right] \quad \text{(A35c)}$$

$$c_4 = \frac{1}{2\gamma_1}e^{-\xi_2}\left[c_1e^{\xi_1}(\gamma_1-1)+c_2e^{-\xi_1}(\gamma_1+1)+\gamma_1\hat{\bar{u}}_D(r_D,1,p)\right] \quad \text{(A35d)}$$

$$c_5 = \frac{1}{2\gamma_2}\left[c_1(\gamma_2+1)+c_2(\gamma_2-1)+\gamma_2\hat{\bar{u}}_D(r_D,0,p)\right] \quad \text{(A35e)}$$

$$c_6 = \frac{1}{2\gamma_2}\left[c_1(\gamma_2-1)+c_2(\gamma_2+1)+\gamma_2\hat{\bar{u}}_D(r_D,0,p)\right] \quad \text{(A35f)}$$

$$\begin{aligned}\chi_2 = {} & -2(1+\gamma_1)(1+\gamma_2)\sinh(\xi_1+\theta_1) - 2(1-\gamma_1)(1-\gamma_2)\sinh(\xi_1-\theta_1) \\ & -2(1+\gamma_1)(1-\gamma_2)\sinh(\xi_1+\theta_2) - 2(1-\gamma_1)(1+\gamma_2)\sinh(\xi_1-\theta_2)\end{aligned} \quad \text{(A35g)}$$

In the same way, one can solve the equations using Eqs. (A20)–(A24) and (A27), the results for Case 3 are

$$c_1 = \frac{2}{\chi_3}\left\{\begin{aligned} & \hat{\bar{u}}(r_D,0,p)e^{-\xi_1}\gamma_2\left[(\sinh\theta_2-\sinh\theta_1)\gamma_1+(\cosh\theta_1-\cosh\theta_2)\right] \\ & +\hat{\bar{u}}(r_D,1,p)\gamma_1\left[(\sinh\theta_1-\sinh\theta_2)\gamma_2+(\cosh\theta_1+\cosh\theta_2)\right]\end{aligned}\right\} \quad \text{(A36a)}$$

$$c_2 = -\frac{2}{\chi_3}\left\{\begin{aligned} & 2\hat{\bar{u}}(r_D,0,p)e^{\xi_1}\gamma_2\left[(\sinh\theta_2-\sinh\theta_1)\gamma_1-(\cosh\theta_1-\cosh\theta_2)\right] \\ & +2\hat{\bar{u}}(r_D,1,p)\gamma_1\left[(\sinh\theta_1-\sinh\theta_2)\gamma_2-(\cosh\theta_1+\cosh\theta_2)\right]\end{aligned}\right\} \quad \text{(A36b)}$$

$$c_3 = \frac{1}{2\gamma_1}e^{-\xi_2}\left[c_1e^{\xi_1}(\gamma_1+1)+c_2e^{-\xi_1}(\gamma_1-1)+\gamma_1\hat{\bar{u}}_D(r_D,1,p)\right] \quad \text{(A36c)}$$

$$c_4 = \frac{1}{2\gamma_1}e^{-\xi_2}\left[c_1e^{\xi_1}(\gamma_1-1)+c_2e^{-\xi_1}(\gamma_1+1)+\gamma_1\hat{\bar{u}}_D(r_D,1,p)\right] \quad \text{(A36d)}$$

$$c_5 = \frac{1}{2\gamma_2}\left[c_1(\gamma_2+1)+c_2(\gamma_2-1)+\gamma_2\hat{\bar{u}}_D(r_D,0,p)\right] \quad \text{(A36e)}$$

$$c_6 = \frac{1}{2\gamma_2}\left[c_1(\gamma_2-1)+c_2(\gamma_2+1)+\gamma_2\hat{\bar{u}}_D(r_D,0,p)\right] \quad \text{(A36f)}$$

$$\begin{aligned}\chi_3 = {} & -2(1+\gamma_1)(1+\gamma_2)\cosh(\xi_1+\theta_1) + 2(1-\gamma_1)(1-\gamma_2)\cosh(\xi_1-\theta_1) \\ & -2(1+\gamma_1)(1-\gamma_2)\cosh(\xi_1+\theta_2) + 2(1-\gamma_1)(1+\gamma_2)\cosh(\xi_1-\theta_2)\end{aligned} \quad \text{(A36g)}$$

https://doi.org/10.5194/hess-2020-586
Preprint. Discussion started: 10 December 2020

Finally, substituting the obtained coefficients for various cases above into Eq. (A21) – Eq. (A23) respectively, and performing inverse Hankel transform can be, after some mathematical manipulation details, written in Eqs. (29) – (37). So far, semi-analytical solutions in the pumped and unpumped layers are derived.

REFERENCES

Bakker M (2013) Analytic modeling of transient multi-layer flow. In: Mishra P, Kuhlman KL (eds) Recent advances in hydrogeology. Springer, Heidelberg

Chen, C., Wen, Z., Zhou, H., Jakada, H., 2020. New semi-analytical model for an exponentially decaying pumping rate with a finite-thickness skin in a leaky aquifer. J. Hydrol. Eng., 25(8): 04020037.

Cihan A, Zhou Q, Birkholzer JT (2011) Analytical solutions for pressure perturbation and fluid leakage through aquitards and wells in multi-layered aquifer systems. Water Resour Res 47(10):W10504. doi:10.1029/2011WR010721

De Hoog, F.R., Knight, J.H., Stokes, A.N., 1982. An improved method for numerical inversion of Laplace transforms. SIAM J. Sci. Stat. Comput. 3 (3), 357–366.

Feng, Q., Zhan, H., 2015. On the aquitard–aquifer interface flow and the drawdown sensitivity with a partially penetrating pumping well in an anisotropic leaky confined aquifer. J. Hydrol. 521, 74–83.

Feng, Q., Zhan H., 2016. Integrated aquitard-aquifer flow with a mixed-type well-face boundary and skin effect. Adv. Water Resour. 89, 42–52.

Feng, Q., Yuan, X., Zhan H., 2019. Flow to a partially penetrating well with variable discharge in an anisotropic two-layer aquifer system. J. Hydrol. 578, 124027.

Feng Q., Luo Y., Zhan H., 2020. Three-dimensional response to a partially penetration well pumping in a

https://doi.org/10.5194/hess-2020-586
Preprint. Discussion started: 10 December 2020

Hydrology and Earth System Sciences Discussions
Open Access

general anisotropic three-layer aquifer system, Journal of Hydrology, 2020, 585, 124850.

Hantush, M.S., 1960. Modification of the theory of leaky aquifers. J. Geophys. Res. 65 (11), 3713–3725.

Hantush, M.S., 1964a. Hydraulics of wells. Adv. Hydrosci. 1, 281–432.

Hantush, M.S., 1964b. Drawdown around wells of variable discharge. J. Geophys. Res. 69 (20), 4221–4235.

Hantush, M.S., 1966. Wells in homogeneous anisotropic aquifers. Water Resour. Res. 2 (2), 583 – 590.

Hantush, M.S., 1967. Flow to wells in aquifers separated by a semipervious layer. Journal of Geophysical Research, 72(6), 1709–1720.

Hemker, C.J., Maas, C., 1987. Unsteady flow to wells in layered and fissured aquifer systems. J Hydrol 90(3 – 4), 231 – 249.

Hunt B., 2005. Flow to vertical and non-vertical wells in leaky aquifers. ASCE J. Hydrol. Engineering, 10 (6), 477–484.

Jeong, J., Park, E., 2019. Comparative applications of data-driven models representing water table fluctuations. J. Hydrol. 572, 261–273.

Lin, Y., Huang, C., Yeh, H., 2019. Analysis of unconfined flow induced by constant rate pumping based on the lagging theory. Water Resour. Res. 55. https://doi.org/10.1029/2018WR023893

Liang, X., Zhan, H., Zhang, Y.K., 2018. Aquifer recharge using a vadose zone infiltration well. Water Resour. Res. 54, 8847–8863.

Loudyi, D., Falconer, R.A., Lin, B., 2007. Mathematical development and verification of a non-orthogonal finite volume model for groundwater flow applications. Adv. Water Resour. 30 (1), 29–42.

Louwyck, A., Vandenbohede, A., Bakker, M., Lebbe, L., 2012. Simulation of axi-symmetric flow towards wells: afinite-difference approach. Comput. Geosci. 44, 136–145.

https://doi.org/10.5194/hess-2020-586
Preprint. Discussion started: 10 December 2020

Mishra, P.K., Vessilinov, V., Gupta, H., 2013. On simulation and analysis of variable-rate pumping tests. Groundwater 51 (3), 469 ‐ 473.

Moench A.F., 1985. Transient flow to a large-diameter well in an aquifer with storative semiconfining layers. Water Resour. Res. 21 (8), 1121–1131.

Mohanty, S., Jha, M.K., Kumar, A., Panda D.K. 2013. Comparative evaluation of numerical model and artificial neural network for simulating groundwater flow in Kathajodi ‐ Surua Inter-basin of Odisha, India. J. Hydrol. 495, 38-51.

Neuman, S.P., 1968. Transient Flow of Ground Water to Wells in Multiple-Aquifer Systems. Ph.D. diss., Department of Civil Engineering, University of California, Berkeley, California.

Neuman, S.P., 1974. Effect of partial penetration on flow in unconfined aquifers considering delayed gravity response. Water Resour. Res. 10 (2), 303–312.

Ogata, H., 2005. A numerical integration formula based on the Bessel functions. Publications of the Research Institute for Mathematical Sciences, 41(4), 949–970.

Rahman, A. T. M. S., Hosono, T., Quilty, J. M., Das, J., & Basak, A., 2020. Multiscale groundwater level forecasting: Coupling new machine learning approaches with wavelet transforms. Adv. Water Resour. 141, 103595.

Rühaak, W., Rath, V., Wolf, A., Clauser, C., 2008. 3D finite volume groundwater and heat transport modeling with non-orthogonal grids using a coordinate transformation method. Adv Water Resour 31(3), 513–524.

Sepúlveda, N., 2008. Three-dimensional flow in the storative semiconfining layers of a leaky aquifer. Ground Water, 46(1), 144–155.

Sen, Z., Altunkaynak, A., 2004. Variable discharge type curve solutions for confined aquifers. J. Am. Water

https://doi.org/10.5194/hess-2020-586
Preprint. Discussion started: 10 December 2020

Hydrology and Earth System Sciences
Open Access
Discussions

Resour. Assoc. 40 (5), 1189–1196.

Singh, S.K., 2009. Drawdown due to temporally varying pumping discharge: inversely estimating aquifer parameters. J. Irrigation Drainage Eng. 135 (2), 257-260.

Theis, C.V., 1935. The relation between the lowering of the piezometric surface and the rate and duration of discharge of a well using ground-water storage. Trans. Am. Geophys. Union. 16, 519–524.

Wang, Q., Zhan, H., Wang, Y., 2015. Non-Darcian effect on slug test in a leaky confined aquifer. J. Hydrol. 527, 747–753.

Wen, Z., Zhan, H., Huang, G., Jin, M., 2011. Constant-head test in a leaky aquifer with a finite-thickness skin. J. Hydrol. 399 (3–4), 326–334.

Wen, Z., Zhan, H., Wang, Q., 2013. Approximate analytical and numerical solutions for radial non-Darcian flow to a well in a leaky aquifer with wellbore storage and skin effect, Int. J. Numer. Anal. Met. 37(11), 1453–1469.

Wen, Z., Zhan, H., Wang, Q., Liang, X., Ma, T., & Chen, C., 2017. Well hydraulics in pumping tests with exponentially decayed rates of abstraction in confined aquifers. J. Hydrol. 548, 40 – 45.

Yeh, H.D., Chang, Y.C., 2013. Recent advances in modeling of well hydraulics. Adv. Water Resour. 51, 27–51.

Zhan, H., Bian, A., 2006. A method of calculating pumping induced leakage. J. Hydrol. 328, 659 – 667.